A STUDY ON POSSIBLE INTERACTIONS

BETWEEN

BIOMOLECULES AND NANOPARTICLES

A Thesis Submitted to the College of

Graduate Studies and Research

In Partial Fulfillment of the Requirements

For the Degree of Master of Science

In the Department of Chemistry

University of Saskatchewan

Saskatoon

By

Amir Houshang Kavianpour

Keywords: nanoparticles, biomolecules, monolayers, interactions, electrochemistry, impedance

PERMISSION TO USE

Presenting this thesis in partial fulfillment of the requirements for a degree of Master of Science from the University of Saskatchewan, I agree that the libraries university may make it available for inspection. I further agree that permission for copying of this thesis in any manner, in whole or in part, for scholarly purposes may be granted by the professor who supervised my thesis work, or in his absence, by the Head of the Department of Chemistry or the Dean of the College of Graduate Studies and Research. It is understood that any copying or publication or use of this thesis or parts thereof, for financial gain shall not be allowed without my written permission. It is also understood that due recognition shall given to me and to the University of Saskatchewan in any scholarly use which may be made of any material in this thesis.

Requests for permission to copy or to make other use of material in this thesis in whole or parts should be addressed to:

Head of the Department of Chemistry

University of Saskatchewan

Saskatoon, Saskatchewan

S7N 5C9

Abstract

Along with the rapid growth of the nanotechnology, nanoparticles (NPs) have found many applications in commercial products. However, there are only a few studies on the toxicity and the environmental effects of NPs in biological systems.

In the study described in this thesis, I have used water-soluble Au NPs that were synthesized using the Brust method and then modified by small molecules. I explored the interactions of these modified Au NPs with self-assembled monolayer films on gold surfaces.

Three types of self-assembled monolayer (SAM) modified gold surfaces were used in this study. The surfaces had SAMs that could be positively or negatively charged or carry no charge, or be able to engage in hydrogen bonding.

Cyclic voltammetry (CV) was used to characterize SAMs of disulfide-glycine conjugate, disulfide-aspartic conjugate, and 11-mercaptoundecanoic acid (MUA) on gold surface electrodes. The possible interactions of Au NPs with the disulfide-aminoacid conjugates and alkanethiol modified surfaces were evaluated by cyclic voltammetry and by electrochemical impedance spectroscopy (EIS). An apparent decline in current density observed in CV along with an electron transfer resistance increase in EIS measurements upon exposure of the films to the MUA-modified anionic Au NPs clearly indicate interactions of the NPs with the films. Likewise, upon exposure of the films to cationic NPs, electron transfer resistance decreases dramatically in EIS experiments. In addition, the current increase in CV measurements provided further evidences for the interactions.

The interactions between modified Au NPs and the SAMs were investigated in more detail by infrared spectroscopy and by employing quartz crystal microbalance. These studies clearly showed that upon exposure of these SAM films to the water-soluble Au NPs, significant changes occur. As would be expected for the adsorption of the Au NPs onto the SAMs, the weight of the film increased due to the addition of the NPs on the surface. Moreover, there are significant increases in the carbonyl stretching vibration at 1735 cm^{-1} along with the appearance of the amide hydrogen stretching band, between 3160-3380 cm^{-1}, which indicate the adsorption of Gly-CSA modified Au NPs onto the MUA film.

ACKNOWLEDGEMENTS

I would like to thank my supervisor, Dr. H.-B. Kraatz,, for all his patience, assistance, support and guidance through the course of this study. His criticisms and suggestions were very instrumental for the successful completion of this work. My gratitude also goes to Advisory Committee, Dr. M. Paige as well as Dr. R. W. J. Scott for helping me to understand various aspects of science. I sincerely thank my lab co-workers, especially S. Chowdhury , and H. Mandal who were very cooperative as chemist, and friend. The assistance given by Dr. K. Brown (NMR) and Mr. K. Thoms (MS) for data collection is also greatly appreciated.

TABLE OF CONTENTS

LIST OF FIGURES AND SCHEMES

LIST OF TABLES

LIST OF ABREVIATION

Asp	aspartic
Boc	*t*-butoxycarbonyl
Bz	benzyl
Calc.	calculated
Cp	cyclopentadien
Cp_{subst}	substituted cyclopentadien
$Cp_{unsubst}$	unsubstituted cyclopentadien
CSA	cystamine
CV	cyclic voltammetry
δ	chemical shift
DNA	deoxyribonucleic acid
E_f	formal potential
$E_{1/2}$	half-wave potential
EDC	1-ethyl-3-(3-dimethylaminopropyl) carbodiimide
E_{pa}	potential of anodic peak
E_{pc}	potential of cathodic peak
ET	electron transfer
Et	ethyl
Fc	ferrocene
FTIR	Furrier Transform Infrared Spectrometry
Gly	glycine
HOBT	N-hydroxybenzotriazole
i_{pa}	anodic peak current
i_{pc}	cathodic peak current
Me	methyl
MS	Mass Spectrometry
MW	molecular weight
n	number of electron
NEt_3	triethylamine
NMR	Nuclear Magnetic Resonance
Ox	oxidized
Ph	phenyl
ppm	parts per million
RAIRS	Reflectance Absorbance Infrared Spectroscopy
Red	reduced
SAM	self-assembled monolayer
TBAP	tetrabuthylammonium perchlorate
tert.	tertiary
TFA	trifluoroaceticacid
TLC	thin layer chromatography

1. Introduction

Nanoparticles are essential components of nanotechnology, is recognized as one of the most promising and latest technologies of in the 21st century. Atoms and molecules in the size range of angstrom, and bulk materials of micrometer size or larger on the other hand, were studied and well understood. However, the respective materials on the nanometer scale fall in between these limits and exhibit interesting properties. Recent studies show that the properties of a material that is nanometer in size is dependent on its size and shape, which is due to the interface and electronic confinement. Since, the ratio of the atoms located on the surface of the materials in this scale is much higher than that of in the bulk materials, the interface causes new and unique properties which are not observed in bulk or individual atoms.[1]

Some nanoparticles have been present in nature or were man-made for thousands of years. Two well known examples are the fullerenes present in soot and gold nanoparticles present in some Roman glass. It was discovered that soot contains buckminster-fullerenes, also known as buckyballs. This family of carbon nanoparticles consists of the well known C_{60} and C_{70} plus other fullerens.[2,3] Their properties and applications are currently being investigated. Another well-known example of nanoparticles are the particles in the Lycurgus cup, which possesses colloidal gold particles within the silica matrix turning the glass ruby-red when light shines through the glass.[4]

More recently, nanoparticles have been made by a variety of techniques, which will be described as part of this introduction and have found applications in areas ranging from sun screen to medical diagnostics.

Applications in the field of biotechnology and medicine were reported, such as the use of TiO_2, CdS, and CdSe quantum dots or semiconductor nanocrystals as fluorescent biological labels in *vivo* imaging and diagnostics.[5-7] The advantages such as having a narrow, tunable, symmetric emission spectrum and being photochemically stable make them more applicable compared to conventional fluorophores[1]

Due to their unique and novel properties, nanoparticles have already found some commercial applications. For example, they have been used as ingredients in some food supplements. Nutraceuticals, such as co-enzyme Q10 (ubiquinon) and lutein, are delivered by nanovehicles (~30 nm micelles) to thier targets. This improves the solubility, bioavailability, and protection against oxidation, enzymatic reaction and hydrolysis of the compounds.[8] Recently, computer prepherals have been coated with nanoparticles. For example, IOGEAR's new Wireless Laser Mouse is coated with nanoparticles having antimicrobial properties.[9] The mouse is coated with a titanium dioxide and silver nano-particle compound. Another example is skin care products from Zinclear containing ZnO nanoparticles, which give protection against broad spectrum UV wavelengths of sun light and show a high transparency for the visible part.[10]

1.1. Nanoparticles, Environment and Human Health Concerns

While there is active research into the applications of nanoparticles, they will potentially find entry poits into daily life. Thus, people will be exposed to NPs in the environment at an ever increasing level. This raises questions as to the environmental impact of NPs. Are they toxic to towards organisms? To date, little is known about the physicochemical properties of nanoparticles in living systems. In fact, some authors

claim that NPs are highly toxic.[11,12] Toxicity of some nanoparticles has been reported while they are known to be less toxic or even harmless in their bulk state. The investigations reported on the toxicity of some fine particles (in the μm scale) compared with ultra-fine particles or nanoparticles in rat models showed an enhanced lung inflammation, fibrosis, and tumor responses in the case of nanoparticles.[11-13] Some documents showed that diseases such as silicosis, asbestosis and black lung have been associated with the interaction of tiny particles with cells and tissues.[12,14,15] Not only the nanoparticles themselves might have some toxicity effects, but also the surface coatings on the nanoparticles may potentially increase the toxicity. For example, Warheit *et al* studied TiO_2 nanoparticles modified with different coatings. The results showed an increase in the toxicity for the nanoparticles containing one of the surface coatings compared to the others.[16] There are many examples which show that nanoparticles can be rapidly taken up by living cells. Wyatt and coworkers showed the uptake of Au nanoparticles modified with different surface coatings, such as cetyltrimethylammonium bromide (CTAB), citrate, and biotin, by human leukemia cells.[17]

1.2. Methods for Nanoparticle Preparation

There are a variety of preparation methods for different NPs reported in the literature. In the following section, common methods of synthesis of semiconductor NPs such as ZnS, CdS, and CdSe as well as preparation of modified Au NPs will be described briefly.

1.2.1. Preparation of Semiconductor NPs (ZnS, CdS, and CdSe)

Murray *et al* [18] applied two methods to prepare Cd semiconductor NPs derivatives, CdX (X = S, Se, Te), in 1993. Both methods consist of adding organometallic reagents into the hot coordinating solvent (100-300 ^{0}C), tri-n-octylphosphine oxide [TOPO]. In method 1, two individually prepared solutions of $CdMe_2$ and TOPX in tri-n-octylphosphine (TOP) are mixed in a glove box and the mixture is then simultaneously injected into the hot solvent. However, the phosphine chalconide precursors used in method 1 are, in the second route, replaced by bis(trimethylsilyl)sulfide $(TMS)_2S$, $(TMS)_2Se$, or bis(*tert*-butyldimethy1silyl) tellurium $(BDMS)_2Te$, respectively. The growth step takes a few hours and results in a size range of 1.2-11.5 nm. To control the size of the nanocrystallites, monitoring the adsorption spectra during the growth step is a common approach. The size may, therefore, be controlled by quenching the reaction, when the desired adsorption observed. The resulted particles have nearly uniform size, shape and surface, in addition to a high degree of monodispersity and consistent crystal structure, which is confirmed by a sharp peak at 450-460 nm at room temperature as well as by the transmission electron microscopy images (Figure 1.1) and X-ray powder diffraction. Since Murray's work, many efforts have been made to find more convenient methods with milder conditions for the preparation. However, the products obtained from his method are still the most stable and monodisperse semiconductor NPs.

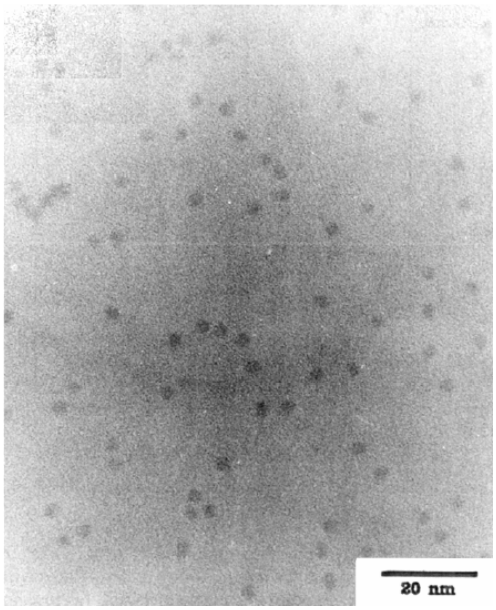

Figure 1.1: TEM image taken in bright field with lattice contrast shows a collection of slightly prolate particles. The elongated (002) axis measures 35.0 Å ± *5%* while the perpendicular axis measures 30 Å ± *6%.* The particles are well dispersed and not aggregated.(Reproduced with the permission from Murray, C. B. et al. *J. Am. Chem. Soc.* **1993**, *115*, 8706-8715. Copyright ©1987 American Chemical Society)

Room temperature synthesis of nanocrystalline CdS, ZnS, and $Cd_xZn_{(1-x)}S$ was reported by Wang *et al*[19] in 2002. They performed a simple and easy chemical reduction of $CdCl_2$, and $ZnCl_2$ in the presence of KBH_4 as a reducing reactant. The process starts by adding a stoichiometric amount of anhydrous $CdCl_2$ or $ZnCl_2$ to an already prepared colorless mixture of sulfur in tetrahydrofuran. The resulting white suspension turns light yellow by adding KBH_4 powder at room temperature. The yellow precipitate formed after 12 h stirring was then purified and characterized by X-ray diffraction, TEM, and UV-vis absorption, which confirmed formation of NPs. However, the same procedure using $ZnCl_2$ or stoichiometric ratios of anhydrous $ZnCl_2$ and $CdCl_2$ powders results in ZnS or $Cd_xZn_{(1-x)}S$ particles, respectively, in a size range of 4-8 nm.

1.2.2. Preparation of Modified Au NPs

Brust *et al* reported a synthesis method for preparation of thiol-modified Au NPs using a two phase liquid-liquid system in 1994.[20] In the two phase system, an aqueous solution of hydrogen tetrachloroaurate ($HAuCl_4$) is added to a solution of tetraoctylammonium bromide in toluene and is vigorously stirred to transfer all the $AuCl_4^-$ into the organic layer. The alkanethiol is then added to the organic phase followed by slow addition of $NaBH_4$ while the mixture is vigorously stirred for about 3 h. Brusts' Au NPs are highly monodisperse and possess a high stability. In this method $AuCl_4^-$ is transferred into the organic phase during its reduction reaction by sodium borohydride by the help of tetraoctylammonium bromide. In this way, the surface reaction with the thiol self-assembled monolayer is gradually and simultaneously carried out when the metal nuclei are growing. The overall reaction is summarized as follows:

$$AuCl_4^-(aq) + N(C_8H_{17})_4 + (C_6H_5Me) \rightarrow N(C_8H_{17})_4^+ AuCl_4^-(C_6H_5Me) \quad (1)$$

$$m\ AuCl_4^-(C_6H_5Me) + nC_{12}H_{25}SH(C_6H_5Me) + 3m\ e^- \rightarrow 4Cl^-(aq) + (Au)_m(C_{12}H_{25}SH)_n(C_6H_5Me) \quad (2)$$

Brust, in his later work, reported a modified strategy for the preparation of mercaptophenol-modified Au NPs, [21] in which a single phase system was used in order to avoid extraction of *p*-mercaptophenol into the alkaline aqueous phase. In this case, $NaBH_4$ was added in small portions to the methanolic solution of $AuCl_4^-$ and thiol, and was stirred vigorously for half an hour. The disappearance of the S-H stretching

vibration in the IR is clear evidence for the attachment of the thiol to the Au NPs (Figure 1.2).

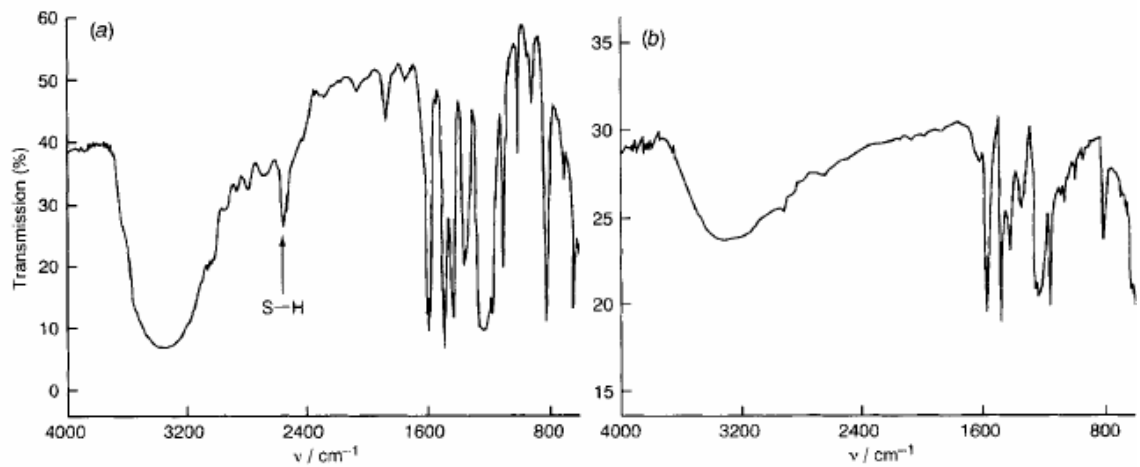

Figure 1.2: IR spectra of (a) *p*-mercaptophenol, (b) NPs modified by *p*-mercaptophenol. The particles were deposited on NaCl disc by evaporation of a drop of an ethyl acetate solution. (Brust, M. *et al. J. CHEM. SOC., CHEM. COMMUN.* **1995**, 1655-1656. Copyright©1995 Reproduced by permission of The Royal Society of Chemistry)

In my thesis, I will work with modified Au NPs, which were prepared by the Brust method.[21] Two capping ligands were used in surface modification of the Au NPs; 11-mercaptoundecanoic acid (MUA) and Boc protected glycinecystamine amino acid conjugate $[Boc\text{-}Gly\text{-}CSA]_2$. The protecting group of the amino functional group in the later NPs was then removed through a deprotection reaction resulting in free amino group among the modified Au NPs. At an appropriate pH (around 7), these NPs were expected to turn into their charged states due to deprotonation of the carboxylic acid functional group in MUA and protonation of the amino functional group in the amino acid conjugate capping ligands.

1.3. Objectives

The toxicity of some nanomaterials and their transportation across cell membrane has already been reported.[5,12,16,17,22] On the other hand, the mechanism and the rate at which nanoparticles can enter cells plus the mode of interaction with biomolecules and potential biological effects are still unknown. Thus, a study on the possible interactions between nanoparticles and some biological molecules such as DNA and proteins is desperately needed.

The objective of this research project is to evaluate possible interactions of nanoparticles with biomolecules in readily manageable model systems. Bio-inspired model systems will avoid some of the complexities of naturally occurring biomolecules. For this purpose, in my thesis I am exploring the interactions of self-assembled monolayer of biomolecules on surfaces exposed to water-soluble nanoparticles.

1.4. Approach

The approach is to monitor the interaction between modified Au nanoparticles and surfaces. Both, the Au NPs as well as the surfaces were modified by organic molecules. Modified Au NPs are stable and easy to prepare, as was shown in Section 1.2.2. Two different molecules, 11-mercaptoundecanoic acid (MUA) and the amino acid conjugate $[Boc\text{-}Gly\text{-}CSA]_2$, were used to prepare modified Au NPs, giving rise to "monolayer protected clusters" or MPCs. The interactions were studied by electrochemical techniques such as electochemical impedance spectroscopy (EIS), cyclic voltammetry (CV), and quartz crystal microbalance (QCM).

In the following, I will describe the approach used in my study followed by a thorough introduction of some of the techniques used in my research.

1.5. Self-Assembled Monolayers

In my research, I am working with self-assembled films of bioconjugate molecules on gold surfaces. Such surface assemblies are sometimes referred to as self-assembled monolayers (SAMs). In the following, I am providing a brief introduction into the preparation and properties of SAMs.

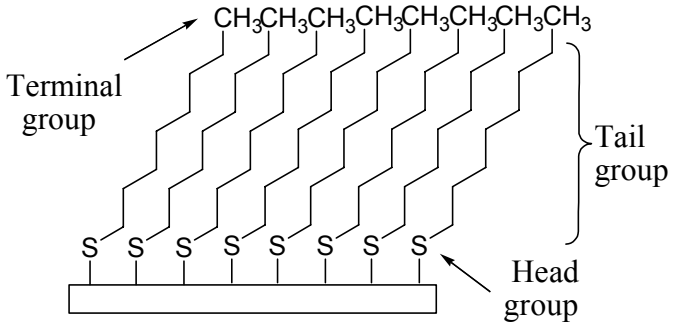

Figure 1.3: A schematic representation of a well organized alkanethiol monolayer on a gold surface in which molecules are close packed with a common orientation

A SAM is an oriented molecular layer adsorbed through chemisorption on a solid surface such as Au, Pt, Al_2O_3 etc. The molecular head groups are attached to the atoms of solid surface, whereas the terminal group is pointing towards the solution interface (Figure 1.3). A variety of head groups have been described, ranging from thiol and disulfide,[23,24] to carboxylic acids[25,26] and others. The use of a particular headgroup will depend on the surface. For example, well-known head groups suitable for the attachment onto gold include thiols, sulfides, and disulfides, whereas carboxylic acid

group is a more appropriate head group for the attachment on aluminum oxide (Al_2O_3) and silver oxide (Ago). Nuzzo and Allara[23] were pioneers in the study of SAMs of bifunctional thiols, disulfides, and sulfides on metal surfaces, especially on gold. Further studies by Whitesides and coworkers[27-30] provided insight into the structure of the films and the mechanism of the self-assembly process. In addition, the effects of the solvent and head groups were studied in detail. For example, thiol SAMs have a controllable thickness and their terminal functional groups facing the solution can be altered. It has been demonstrated that the resulted monolayers obtained from chemisorption of alkanethiols and of di-*n*-alkyl disulfides on clean gold are identical,[31] in which the Au(I)-thiolate (RS^-) species are formed. Kinetic studies have revealed two steps for the chemisorption of alkanethiols onto gold surface; the first step involves a very fast (few minutes) redox chemisorption, in which the contact angles reach their limiting values and the thickness is about 80-90% of its maximum, and a slow step afterward (several hours) engages reorganization of molecules among the SAM to achieve its final values of thickness and contact angles.[27,31,32] The overall reactions that are suggested for the adsorption of alkanethoils and dialkyldisulfides are summarized in the following:[31,32]

$$RSH + Au(0) \rightarrow RS^-Au^+ + \tfrac{1}{2} H_2$$

$$RS\text{-}SR + 2\ Au(0) \rightarrow 2\ RS^-Au^+$$

The ability to modify both tail and terminal groups of the molecules makes SAMs excellent systems for investigation of intermolecular interactions such as hydrogen-bond[33] and electrostatic interactions.[34] For example, Zamborini *et al* described

interfacial interactions in formation of monolayer or multilayer nanoparticle films based on electrostatic attractions caused by using Cu^{2+} or Zn^{2+} cations between two anionic species; monolayer protected Au clusters (MPCs) and a mixed SAM consisted of hexanethiolate/mercaptoundecanoic acid ($C_6/C_{10}COOH$).[35] The electrochemical behavior of arrays of Au nanoparticles assembled on Au electrodes modified by 11-mercaptoundecanoic acid (MUA) and poly-L-lysine (PLYS) as a function of particle number density was reported by Zhao *et al*.[36]

1.6. Electrochemistry

As a potential is applied to an electrode, two types of processes, Faradaic and non-Faradaic, occur across the electrode-solution interface. The electron transfer or charge transfer at the interface, which results in an oxidation or reduction reaction of the electroactive species, is called Faradaic process and the resulting current as Faradaic current. This process is controlled by the diffusion of the electroactive species from the bulk solution onto the electrode surface and vise versa. The accumulation of charges will result in a double layer at the interface, through which the external current can at least transiently flow without transferring any charges across the electrode surface. This is named as non-Faradaic process, and the related current flow as to non-Faradaic or charging current. Therefore, any adsorption, desorption of the species at the electrode surface may cause a change in the potential or the solution composition and consequently will change the structure of the interface.

Since the structure of the electrode-solution interface has significant impact on both Faradaic and non-Faradaic processes electrochemical techniques could be

promising methods to study interfacial interactions. For example, an alkanethiol self assembled monolayer on a Au electrode changes the interface such that it can block the species away from the electrode surface. Hence, the resulted signals in the electrochemical measurements, such as maximum current, formal potential, and peak separation in cyclic voltammetry (CV), or charge transfer resistance and double layer capacitance obtained from electrochemical impedance spectroscopy (EIS) will be significantly affected. As a result, the packing structure of a SAM can be explored through the use of electrochemical techniques in presence of electroactive species in the solution.

1.6.1. Cyclic Voltammetry

Cyclic voltammetry (CV) is an easy method to characterize a SAM on an electrode surface and to investigate the interfacial interactions as well. For example, CV studies on the structural properties of n-alkyl thiol SAMs on gold electrode surfaces was reported by Chidsey and coworkers.[37] The CV of the bare electrode in presence of the redox probe, $Fe(CN)_6^{3-}$, shows two oxidation and reduction peaks with separation of about 60 mV and identical areas, which indicate a fully reversible redox reaction (Figure 1.4 (solid line)). However, Faradaic process for the modified or protected electrode by the alkyl thiol is dramatically inhibited. The current measured on the modified electrode using a probe (Figure 1.4 (B-solid line)) is 0.01% compared with that of the bare gold electrode (A-solid line). Additionally, the CV measurements at around the redox formal potential ($E_{1/2}$) shows identical amount of current for the modified electrode in the

presence (B-solid line) and in the absence of the redox probe (B-dashed line), which points out there is no Faradaic current for the modified electrode.

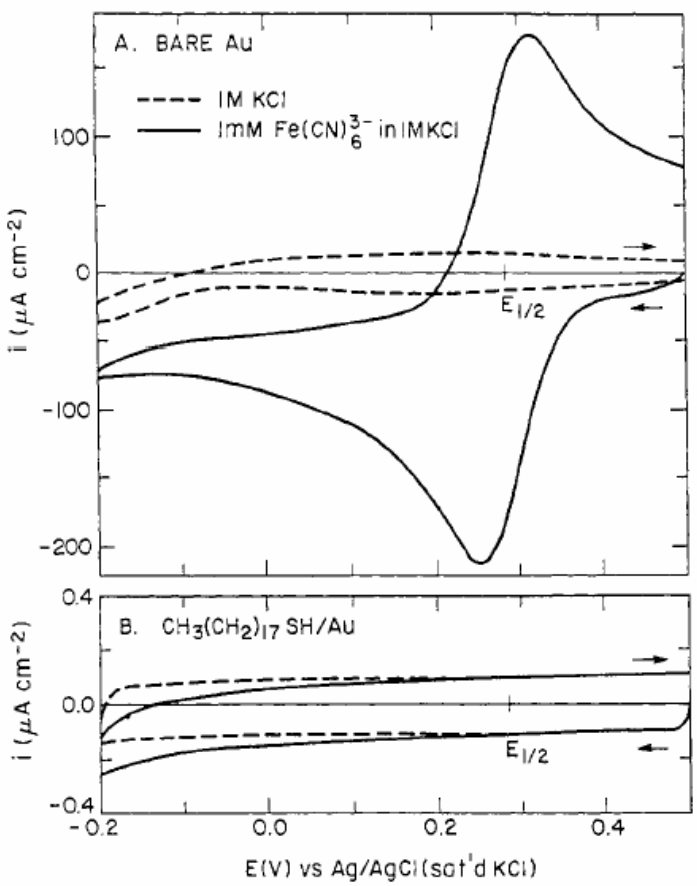

Figure 1.4: Cyclic voltammetric current response vs. applied potential for (A) bare gold and (B) $CH_3(CH_3)_{17}SH$-Au modified electrode. The solutions are 1 rnM $Fe(CN)_6^{3-}$ in 1 M KCI (solid line) and only 1 M KC1 (dashed line). The sweep rate is 100 mV/s. (Reproduced with the permission from Porter, M. D. et al. *J. Am. Chem. Soc.* **1987**, *109*, 3559-3568. Copyright ©1987 American Chemical Society)

The electron transfer process of electroactive probes on different alkyl thiol-modified electrodes was examined using CV technique by Ganesh *et al*[38]. In their study, the effect of chain length on the blocking properties of the SAMs was studied. Alkyl thiols with different chain lengths were prepared and used in the preparation of SAMs on gold electrode. Figure 1.5 is a cyclic voltammogram obtained from electrodes in a solution consisting of $Fe(CN)_6^{3-}$ anions, acting as an electroactive probe. The

voltammogram of the bare gold electrode (a) shows a reversible redox reaction for the probe. However, it seems that the redox reactions of the probe for C_5 and C_{10} thiols coated electrodes were inhibited. The voltammogram demonstrates a trace characteristic of microelectrode arrays[39-41] due to the existence of pinholes among the SAMs, indicating highly compact and ordered monolayers formed on the electrode surfaces.

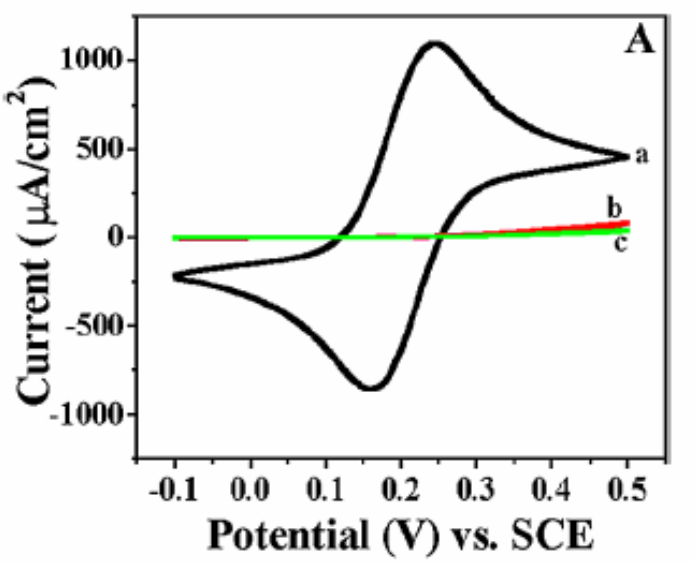

Figure 1.5: CV in 10 mM $K_3[Fe(CN)_6]$ with 1 M NaF as supporting electrolyte at a potential scan rate of 50 mV/s for (a) bare Au electrode, (b) and (c) are the respective SAMs of C_5 and C_{10} alkanethiol on Au. (Reprinted from Ganesh, V. et al. *Journal of Colloid and Interface Science* **2006**, *296*, 195-203. Copyright © 2006 with permission from Elsevier)

In addition, to get more insight into the electron transfer process taking place and the characteristics of the interfacial behavior, a $[Ru(NH_3)]_6Cl_3$ cationic redox probe was also exploited in the same series of CV measurements (Figure 1.6). It can be noted that the C_{10} thiols on the electrode (c) show a well packed and ordered monolayer with small pinholes. Although, C_5 thiol SAM (b) shows quasi-reversible behavior with a large peak-separation and peak current values close to that of the bare gold electrode.

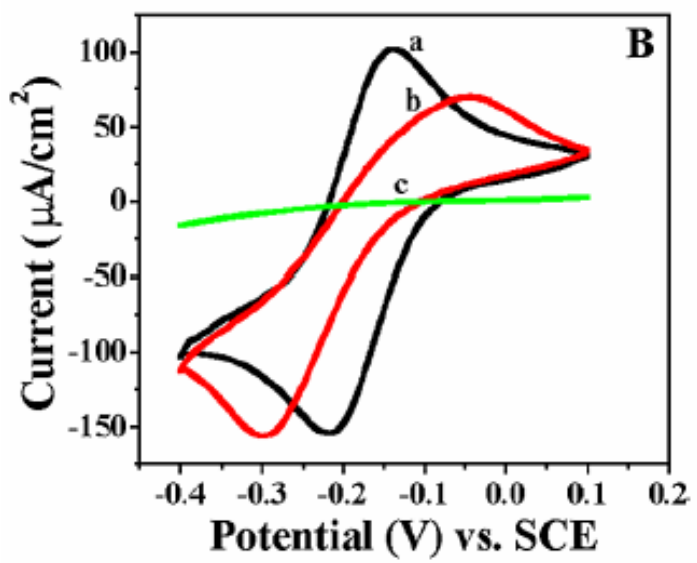

Figure 1.6: CV in 1 mM $[Ru(NH_3)]_6Cl_3$ with 0.1 M LiClO4 as supporting electrolyte at a potential scan rate of 50 mV/s for (a) bare Au electrode, (b) and (c) are the respective SAMs of C_5 and C_{10} alkanethiols on Au. (Reprinted from Ganesh, V. et al. *Journal of Colloid and Interface Science* **2006**, *296*, 195-203. Copyright © 2006 with permission from Elsevier)

Comparing the two conditions for the same SAM (C_5) explains while there is no diffusion controlled electron transfer occurring at the interface in presence of $K_3[Fe(CN)_6]$probe, however, the current observed in presence of $[Ru(NH_3)]_6Cl_3$ redox probe is suggested to result from a tunneling electron transfer through the short alkane chains of the thiols (Figure 1.7).

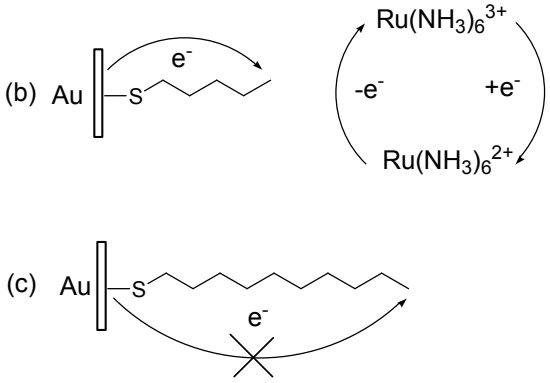

Figure 1.7: Schematic representation of tunneling electron transfer through the alkane chain of the C_5 (b) and C_{10} thiol SAM in presence of [Ru(NH3)6]2+/3+ as redox probes.[37]

1.6.2. Electrochemical Impedance Spectroscopy (EIS)

Electrochemical impedance spectroscopy is a powerful tool for examining many chemical and physical processes in solution as well as in solids. A typical modeling procedure uses electrical circuits that consists of components such as resistors and capacitors to explain the electrochemical behavior of the interface. Changes in the values for the individual components indicate their behavior and performance. Impedance spectroscopy is a non-destructive technique and thus can provide time dependent information about the ongoing processes.

In impedance spectroscopy, a small sinusoidal voltage is applied to the sample over a wide frequency range, which is therefore an alternating current (AC) technique. The magnitude of the current induced by the applied potential and in addition the phase angle between the potential and maximum current are measured. For DC conditions Ohm's law (R = E / I) describes resistance in terms of the ratio between potential E and current I. However, in AC conditions, a sinusoidal potential induces a sinusoidal current as a function of time.

$$E(t) = E_0 \cos(\omega t) \qquad (1.1)$$

$$\omega = 2\pi f \qquad (1.2)$$

where E (t) is the potential at time t, E_o is the amplitude of the signal, and ω is the radial frequency. In a linear or psudo-linear system, both potential and current have the same frequency but they are in different phase, φ (Figure 1.8).

$$I(t) = I_0 \cos(\omega t - \varphi) \qquad (1.3)$$

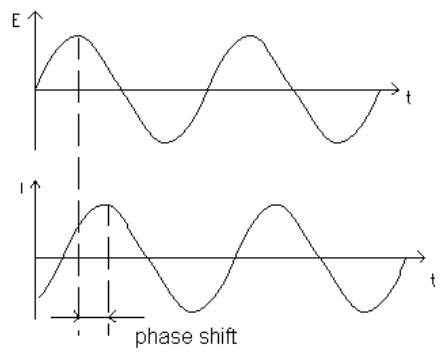

Figure 1.8: Sinusoidal Current Response in a Linear System

Impedance (Z) of the system, which is analogous to resistance in Ohm's law, is defined as the ratio between potential E (t) and I (t):

$$Z = \frac{E(t)}{I(t)} = \frac{E_0 \cos(\omega t)}{I_0 \cos(\omega t - \varphi)} = Z_0 \frac{\cos(\omega t)}{\cos(\omega t - \varphi)} \qquad (1\text{-}4)$$

The impedance is expressed in terms of a magnitude, Z_0, and a phase shift, φ. Using Euler's equation, it is possible to express the impedance as a complex function,

$\exp(j\varphi) = \cos\varphi + j\sin\varphi$

Applying the potential and current as complex expressions,

$E(t) = E_0 \exp(j\omega t)$

$I(t) = I_0 \exp(j\omega t - j\varphi)$

The impedance is then represented as a complex number,

$$Z(\omega) = \frac{E(t)}{I(t)} = Z_0 \exp(j\varphi) = Z_0 (\cos\varphi + j\sin\varphi) \qquad (1.5)$$

The expression for $Z(\omega)$ is composed of a real and an imaginary part. A plot of the imaginary part versus the real part of the measured impedance data is named as a "Nyquist plot" (Figure 1.9).

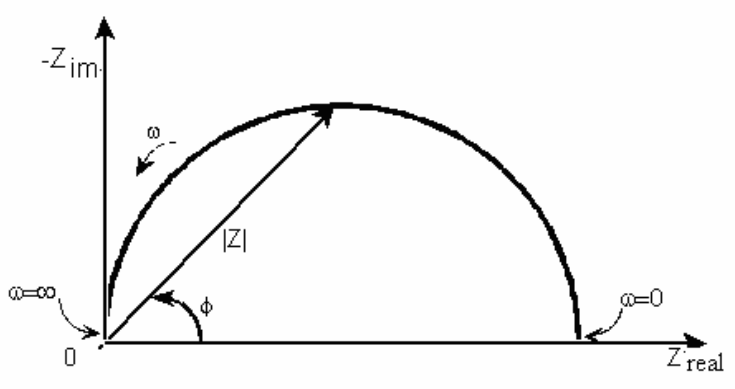

Figure 1.9: A typical Nyquist Plot with Impedance Vector

When the phase angle (φ) is zero, then a pure resistance is present. When a phase angle of 90^{o} is measured, a pure capacitance is present. Angles between these values indicate that a combination of a capacitor and resistor is present. An electrical equivalent circuit is an appropriate approach in which the data can be modeled to provide quantitative values for solution resistance (R_s), double layer capacitance (C_{dl}) and most importantly charge transfer resistance (R_{ct}). For example, equivalent circuit modeled for the data obtained from the Nyquist plot in Figure 1.9 is presented in Figure 1.10. The semicircle is characteristic of a single "time constant".

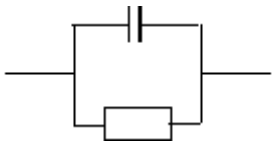

Figure 1.10: Simple Equivalent Circuit with One Time Constant

EIS has attracted many research interests in studying interfacial biomolecular interactions, characterization of the structural features of the interface and the mechanism of the electrochemical processes occurring at the electrode-solution interface.[42-44]

For example, to directly probe and quantify the response of avidin-biotin conjugate, Ding, *et al* [43] applied CV and EIS techniques in a solution of $Fe(CN)_6^{3-/4-}$. The electrodes were initially modified by 11-mercaptoundecanoic acid (MUA). Avidin was then immobilized on the MUA monolayer to be interacted finally with biotin. The obtained CV plots (Figure 1.11 (left)) demonstrate the stepwise formation of modification layers on the electrode surface by presenting less Faradaic current from (a) to (d), respectively. The apparent decline in the Faradaic current accompanied with the immobilizations can be interpreted by the decrease in the rate of the charge transfer process, which is due to the increased thickness of the layers. The CV data was confirmed by EIS measurements, where the semicircles in the Nyquist plots (Figure 1.11 (right)) expand with the adding modifiers from (a) to (d), respectively. As it can be noted, the differences between steps observed in EIS, especially after MUA modification, are much larger than those of in CV, which is clearly indicative of the higher sensitivity of EIS technique compared to CV. Moreover, no Warburg impedance element is observed for the modified electrode in contrast with the bare electrode, which is expected for an immense electron transfer resistance (R_{et}) of the modified electrode. For an electrochemical process with a great R_{et} the diffusion-controlled part can not affect the electron transfer rate. Hence, the Warburg element, which arises from a diffusion-controlled process in low frequency, does no longer appear. Alternatively, for a bare electrode with no barrier on the surface and an obviously small R_{et} the diffusion-controlled process needs to be taken into account and consequently the Warburg component becomes visible.

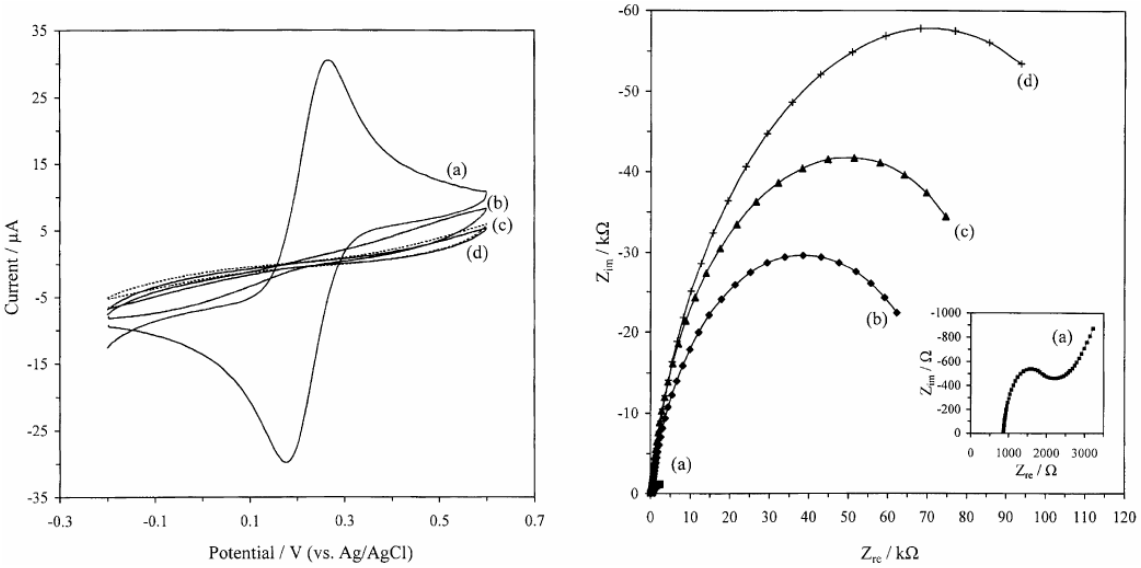

Figure 1.11: CV (left) and Nyquist plots (right) of the bare gold electrode (a) following modification of MUA (b), MUA+ avidin (c), and MUA+ avidin + glycine (d). The supporting electrolyte is 50mM MES containing $Fe(CN)_6^{3-/4-}$ couple. The scan rate in CV is 100 mV/s.[42]

1.8. Thesis Outline

Here, I outline what I will present in the next chapters. In Chapter 2, I present the results of my study into the interaction of modified Au nanoparticles with monolayer surfaces. Section 2.1 outlines the synthesis and characterization of disulfide-amino acid conjugates. Thin films are fully characterized and the results of this study are described in Section 2.2. In particular, I will focus on the electrochemical characterization of the disulfide-amino acid conjugate films on electrode surfaces, as well as the reflectance-absorbance infra-red spectroscopy (RAIRS) and X-ray photoelectron spectroscopy (XPS) characterization for the MUA films. In Section 2.3, the results of my study into the interactions of monolayer protected gold NPs (MPCs) with the biomolecule films on gold electrodes will be discussed in detail.

In Chapter 3, after presenting a short summary of my research achievements, I provide some suggestions for future work in the area of NPs interactions with biomolecules.

2. RESULTS AND DISCUSSION

2.1. Synthesis and Characterization of Disulfide-aminoacid Conjugates

Three peptide disulfides where synthesized as part of this research, ranging from a Boc-protected Gly-cystamine conjugate **1**, to the aspartate-conjugate **2**, to the organometallic ferrocene-conjugate **5**. These systems were designed with a range of "head groups" that enable different interactions with modified gold nanoparticles, as will be briefly illustrated at the end of this section.

[Boc-Gly-CSA]$_2$ (**1**)

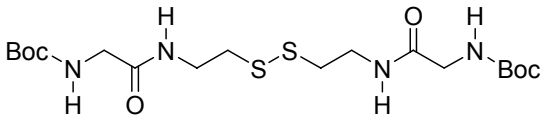

[Boc-Asp(Bz)-CSA]$_2$ (**2**)

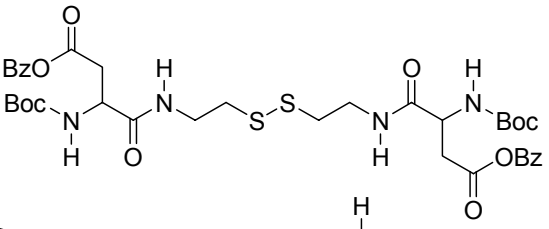

[Fc-Lys(Boc)-CSA]$_2$ (**5**)

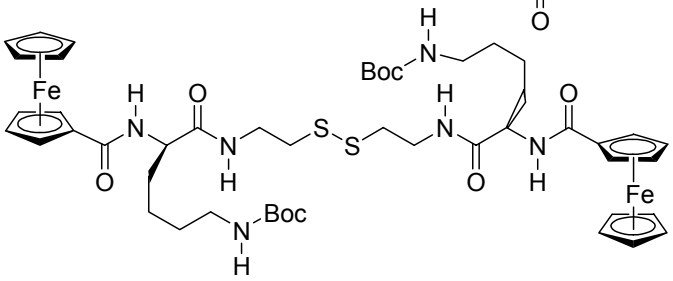

Compounds **1** and **2** were designed to provide access to peptide films that could be converted to charged surfaces. In the case of conjugate **1**, deprotection of the Boc group with trifluoroacetic acid will result in the formation of a positively charged ammonium-terminated surface, while deprotection of the benzyl group by hydrogenation of by base will provide access to carboxylate terminated surfaces. This approach would enable us to probe the interaction of these charged surfaces with modified gold nanoparticles (NPs).

Peptide disulfides **1**, **2**, and **5** were synthesized using the carbodiimide HOBt method.[45-47] Scheme 2.1 shows the synthesis of [Boc-Gly-CSA]$_2$ (**1**) as a general example of the syntheses of this group of compounds. Boc-Gly-OH was reacted *in situ* with the water soluble carbodiimide EDC and 1-hydroxybenzotriazole (HOBT) in dichloromethane. To this reaction mixture, a slurry of cystamine hydrochloride ([CSA]$_2$·2HCl) and triethylamine in dichloromethane were added to produce the desired Boc-protected peptide disulfide **1** in a good yield.

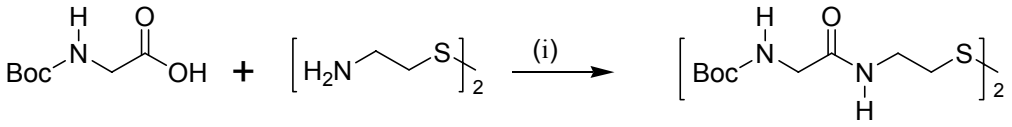

(**1**) Yield = 82%

Scheme 2.1: Schematic representation of the synthesis of [Boc-Gly-CSA]$_2$ (**1**)**.** (i) Conditions: EDC, HOBt, Et_3N in CH_2Cl_2 at 0^{o}C.

Next, the aspartate conjugate **2** was synthesized from Boc-Asp(Bz)-OH following the general procedure used for the synthesis of compound **1**.

In order to quantify the amount of peptide linked to electrode surface, it was decided to prepare the Lys-ferrocene (Lys-Fc) conjugate **5**. This molecule possesses the redox active Fc group, a well known electrochemical probe,[48] which enables the quantification of peptide molecules on surfaces and determines the surface concentration and extracts the molecular footprint, as long as the geometric surface area of the electrode is known. Furthermore, the Fc group may also serve as a probe enabling the quantification of the surface concentration for the film before and after Boc-deprotection

of lysine. The synthesis of the Fc-Lys conjugate **5** from Fc is summarized in Scheme 2.2.

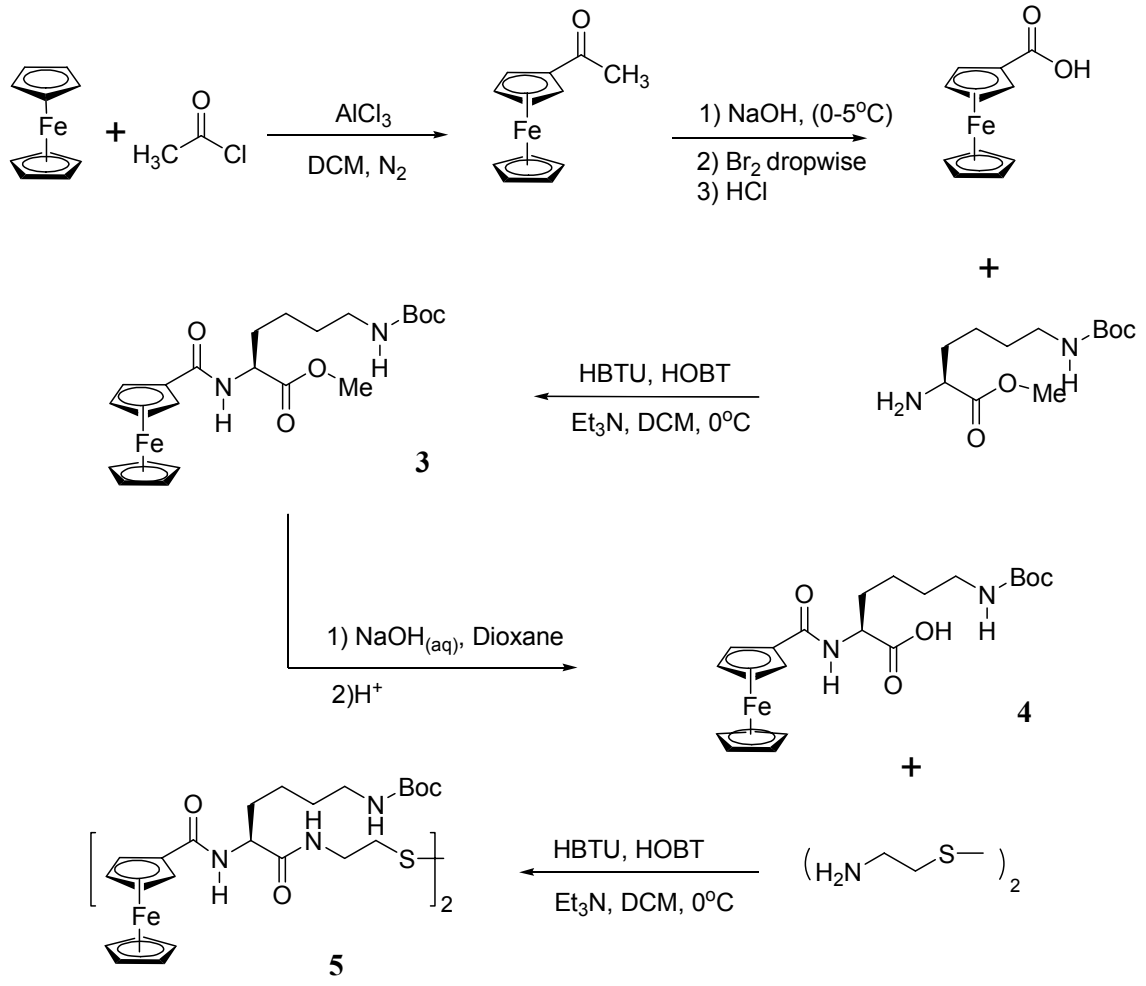

Scheme 2.2: Synthetic steps in preparation of compound **5**

Scheme 2.2 displays the synthetic steps applied in preparation of compound **5**. Starting from Fc, the acid Fc-COOH was obtained by acetylation of Fc,[49,50] followed by oxidation in the presence of Br_2/NaOH. Reaction of Fc-COOH with group Lys(Boc)-OMe using carbodiimide coupling, results in the formation of compound **3**. After base hydrolysis, the free acid Fc-Lys(Boc)-OH (**4**) is coupled with cystamine hydrochloride to give the desired disulfide **5**.

Selected ^{1}H and $^{13}C\{^{1}H\}$-NMR spectroscopic features for peptide disulfides **1, 2,** and **5** are summarized in Table 2.1. The ^{1}H-NMR assignments were made based on chemical shift, relative integration and signal multiplicity.

Table 2.1: ^{1}H and $^{13}C\{^{1}H\}$-NMR Chemical Shifts (δ) for compounds **1**, **2** and **5** in $CDCl_3$ at a concentration of 2 mM.

	^{1}H-NMR (δ = ppm)					^{13}C-NMR (δ = ppm)				
	NH (CSA)	NH (Amino acid)	H^{α} (Amino acid)	H^{β} (CSA)	H^{α} (CSA)	CO (Amino acid)	CO (Boc)	C^{α} (Amino acid)	C^{β} (CSA)	C^{α} (CSA)
1	6.90	5.50	3.85	3.60	2.85	170.6	156.6	44.8	38.9	38.4
2	7.03	5.80	4.56	3.52	2.77	171.9	155.9	44.8	38.8	36.6
5	7.55	7.05	4.92	3.45	2.82	173.3	156.5	52.8	38.8	38.2

^{1}H-NMR spectra of compounds **1**, **2**, and **5** in $CDCl_3$ are displayed in Figure 2.1. The resonances for the amide protons for all three compounds were observed between δ5.50 and δ7.55. The NHs connected to the cystamine (CSA) were observed further down-field, in the region of δ6.90-7.55, whereas the NHs connected to the Boc group were found in the region of δ5.80 to δ5.1.

The methylene protons of cystamine for all three compounds were observed as two distinct sets of signals. For compound **1**, the CH_2 protons were observed as two broad singlet signals, while for **2** and **5**, the appearance of these signals is distinctly different. For example, the CH^{β}_2 of the cystamine group for compound **2** is split into two signals, each for one of the two diastereotopic protons of the CH_2 group.

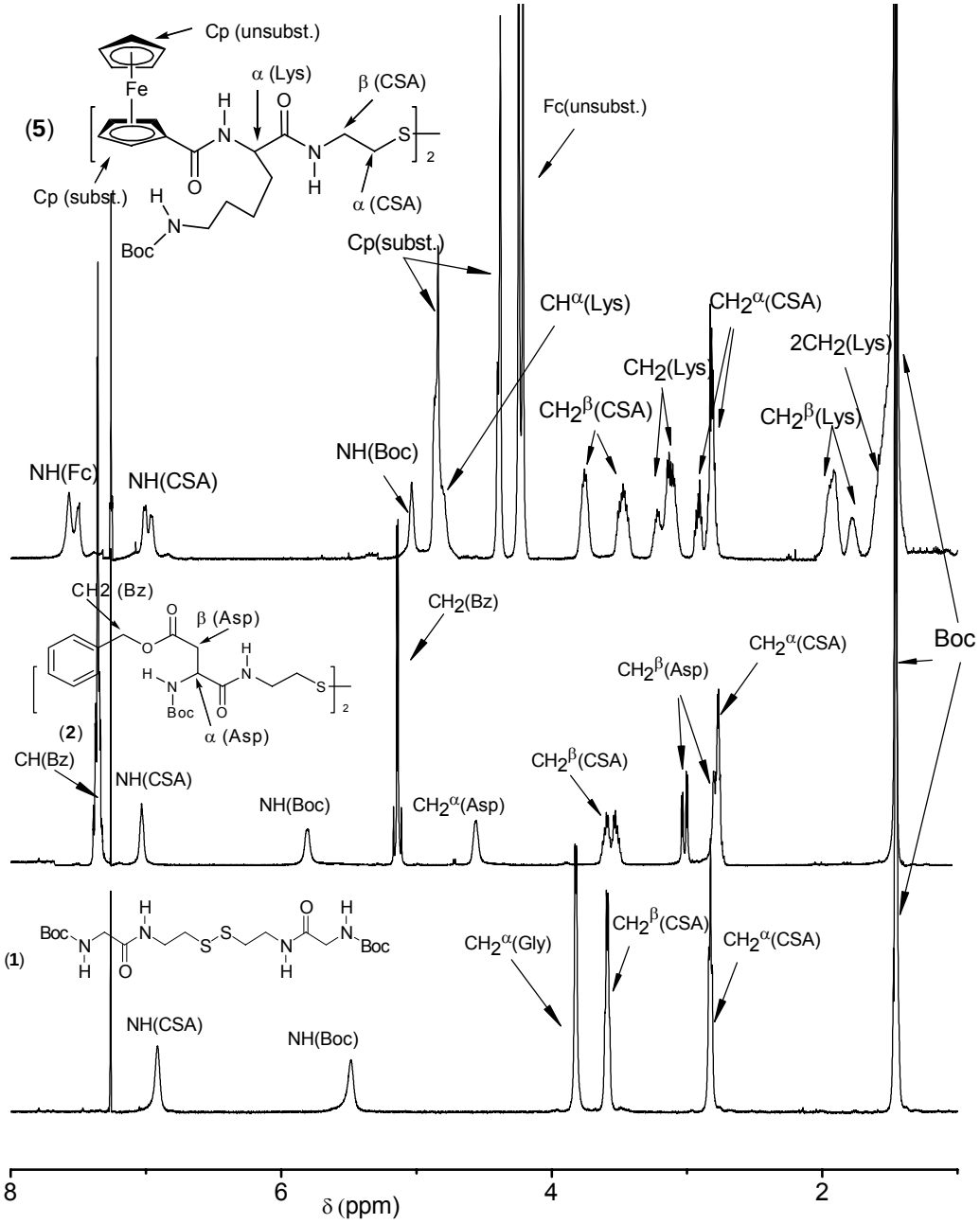

Figure 2.1: ^{1}H-NMR spectra in the range of 8 – 1 ppm for compounds **1**, **2**, and **5**. The spectra were recorded in $CDCl_3$ and were referenced against the residual signal for $CHCl_3$ at δ7.23.

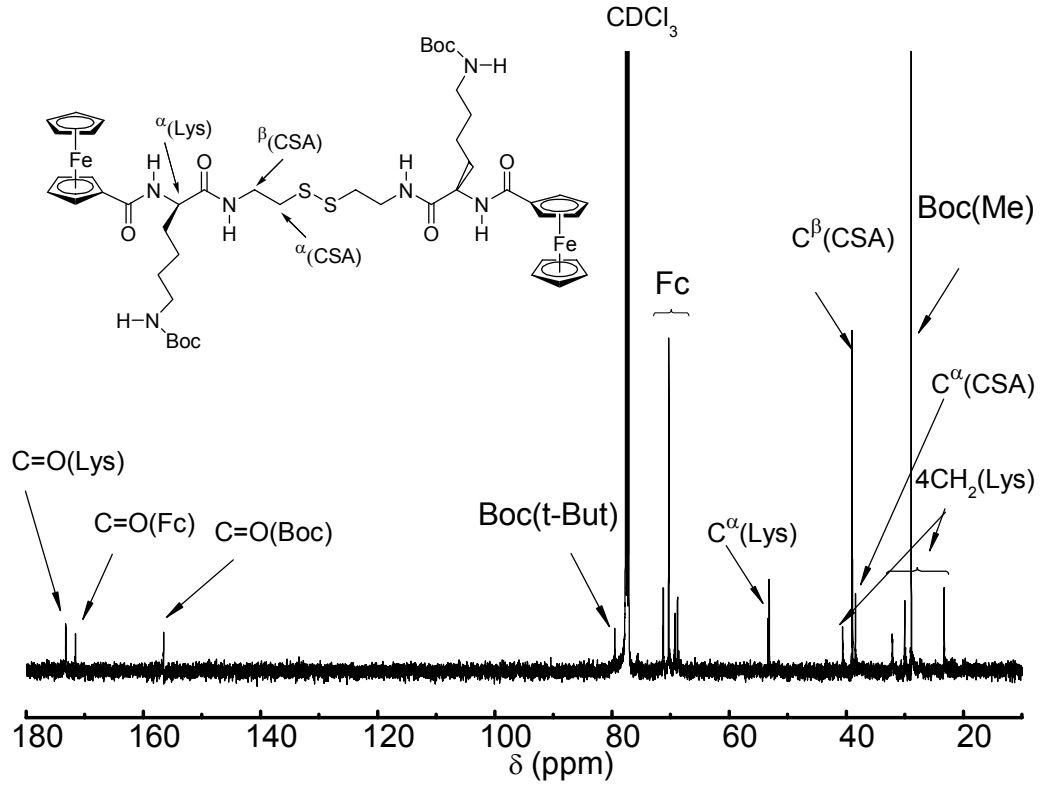

Figure 2.2: $^{13}C\{^{1}H\}$-NMR spectrum of compound **5** in $CDCl_3$

.

The $^{13}C\{^{1}H\}$-NMR and ^{1}H-NMR spectra of compounds **1**, **2** and **3** are found in the appendix. As an example, the $^{13}C\{^{1}H\}$-NMR spectrum of compound **5** recorded in $CDCl_3$ is shown in Figure2.2. The three signals in the carbonyl region of the spectrum at δ 173.8, 171.9, and 156.6 ppm were assigned to the C=O groups of lysine, ferrocene and Boc, respectively. These compared well with the chemical shift of other Fc-CO and Boc-CO groups.[51] One signal for the unsubstituted Cp ring was observed at δ 68.9, and three signals for the substituted Cp ring of ferrocene group were observed at δ 69.3 (CH_m Cp), 70.3 (CH_o Cp), 71.3 (C Cp), respectively. These compared well with the chemical shift of Cp rings of Fc-peptide conjugates reported earlier.[51,52] The tertiary carbon and Boc-methyl groups gave signals at δ 79.7 and 28.9, respectively.[51]

Due to the redox active Fc group, compound **5** was also characterized electrochemically by cyclic voltammetry. Figure 2.3 shows a typical cyclic voltammogram (CV) of a 1 mM solution of compound **5** in acetonitrile in the presence of 0.1 M tetrabutylammonium perchlorate (TBAP) as supporting electrolyte. In the CV, the conjugate **5** exhibits a fully reversible one-electron oxidation, with a half-wave potential $E_{1/2}$ of 600 (±5) mV *vs* Ag/AgCl, which is typical of Fc-amino acid conjugates which have $E_{1/2}$ in the range of 450-700 mV *vs* Ag/AgCl.[53]

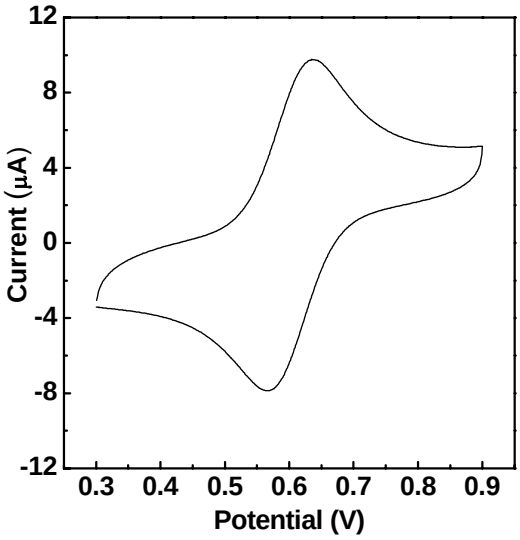

Figure 2.3: Cyclic voltammogram of compound **5** in acetonitrile solution (1 mM). Scan rate: 100 mVs^{-1}, 0.1 M TBAP in MeCN, glassy carbon working electrode, Ag/AgCl as a reference and Pt wire as counter electrode.

However, all efforts made to prepare well formed films of compound **5** failed due to instability of the film on the surface. Therefore, no result from experiments related to film preparation and interaction with nano-particles (NPs) for compound **5** is presented in our study.

2.2. Preparation of Films on Gold Surfaces

This chapter begins with a brief description of the rigorous cleaning procedures used for cleaning gold electrodes and is then followed by a discussion of the film preparation for peptide films and binary films of 11-mercaptoundecanoic acid (MUA)-decanethiol (DT) on polycrystalline gold surfaces.

2.2.1. Preparation of Gold Electrodes

In order to avoid having any physically and chemically adsorbed contaminants on the surfaces, all electrodes were cleaned prior to surface modification. To have a smooth surfaces, the gold electrodes (Bioanalytical Systems, Inc., 1.6 mm diameter) were polished using a slurry of alumina powder (0.3 μm, 0.1 μm, and 0.05 μm in diameter, sequentially), rinsed with Milli-Q water, and then sonicated in ethanol for 1 minute. Next, the electrodes were cleaned electrochemically by linear sweep voltammetry (LSV) in a solution of KOH (0.5 M) in the potential window of 0.0 to -1.5 V *vs* Ag/AgCl. This allowed the removal of any adsorbed thiolate molecules from the surface. These scans were repeated until no reducing peak was observed in the potential window. Then, the electrodes were subjected to repeated CV scans in sulfuric acid (0.5 M) in a potential window of 0.0-1.6 V *vs* Ag/AgCl at a scan rate of 100 mV/s, until a stable CV was obtained (Figure 2.5).

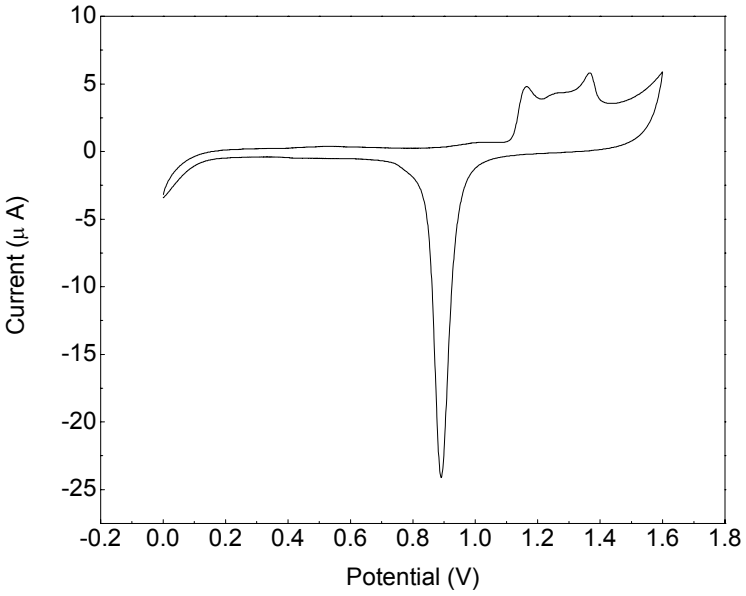

Figure 2.5: A typical stable CV of a bare gold electrode (Bioanalytical Systems, Inc., 1.6 mm diameter) in 0.5 M sulfuric acid solution *vs* Ag/AgCl as reference electrode and platinum wire as counter electrode.

2.2.2. Preparation of Homogeneous and Heterogeneous Films

Homogeneous films of peptide disulfides **1**, **2**, and **5** were prepared by soaking cleaned gold substrates in a 1 mM ethanolic solution of the respective peptide conjugate for five days[45]. Scheme 2.3 demonstrates the formation of monolayer from a solution of a disulfide compound. Disulfides and thiolates covalently bind to gold surfaces through their sulfur atoms[32], resulting in the formation of gold-thiolate linkages[29,37,54,55]. After the self-assembly, the modified gold surfaces were left in Milli-Q water for five to six hours[56] prior to performing any electrochemical experiments.

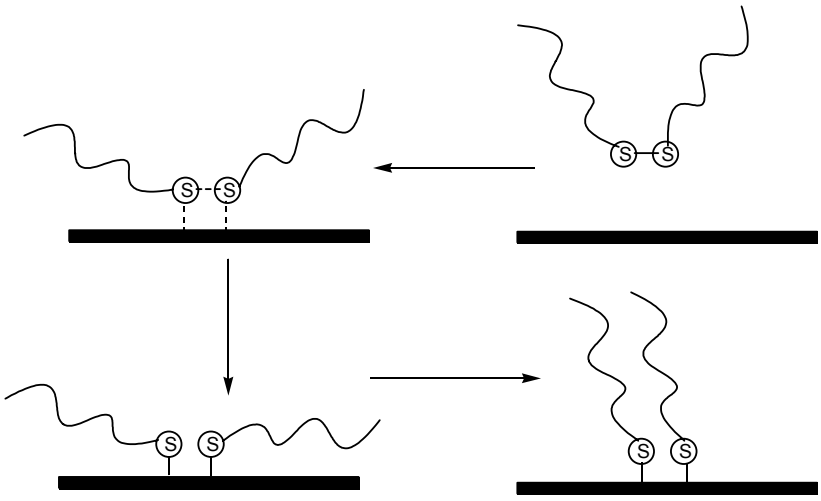

Scheme 2.3: Schematic representation for formation of a disulfide film by self assembly.

For the preparation of heterogeneous films, cleaned gold electrodes were soaked in a solution of mixed alkanethiolates, prepared from MUA and 1-decanethiol (DT) in a ratio of 1:2 resulting in a total thiol concentration of 1 mM in ethanol (Figure 2.6). In order to obtain good and reproducible films, different immersion times were evaluated ranging from 12 hours to two days. However, no difference was apparent in the prepared monolayers. Thus, it was decided to use a 24 hour immersion time for all heterogeneous film preparations in order to standardize the preparation of heterogeneous films.

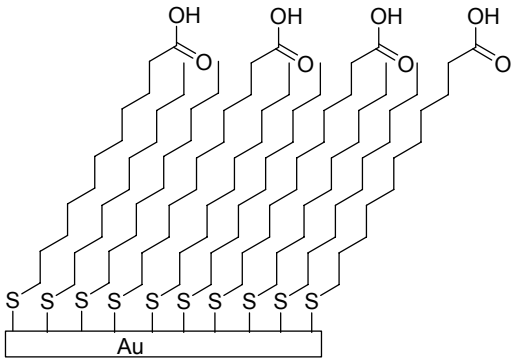

Figure 2.6: Schematic representation of an ideal dilute film prepared from 11-mercaptoundecanoic acid (MUA) and 1-decanethiol (DT) in a 1:2 ratio on a gold surface

2.2.3. Characterization of Films

All films were characterized by cyclic voltammetry (CV), and in some cases, by non-electrochemical techniques such as reflection-absorption IR spectroscopy (RAIRS), and X-ray photoelectron spectroscopy (XPS).

The peptide disulfide **1**, **2**, **5**, and diluted MUA films on gold electrode surfaces were immediately characterized after deposition by CV. An electro-active probe, such as $[Fe(CN)_6]^{3-/4-}$, can be used to probe the quality of the films[43,57] and give information about how well packed the film is and how well the probe molecule can penetrate the film to access the electrode surface (Scheme 2.4). In this particular system, electron transfer takes place between the electro-active probe in solution and the surface. In the absence of a molecular film on the gold surface, the redox reaction is unimpeded. However, in the presence of a well-packed film, oxidation of the Fe(II) is no longer observed since the $[Fe(CN)_6]^{4-}$ cannot access the gold surface and electron transfer through the film is slower.[58]

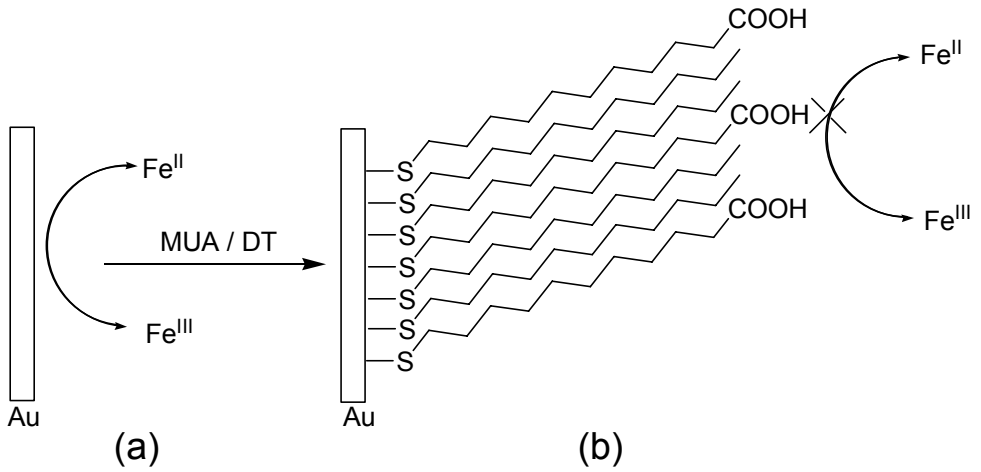

Scheme 2.4: Schematic representation of a typical redox reaction for the $Fe^{II/III}$ redox couple of $[Fe(CN)_6]^{3-/4-}$ on a) a bare gold electrode and b) a gold electrode modified with mixed film of 11-mercaptoundecanoic acid (MUA) and 1-decanethiol (DT) in a 1:2 ratio

A typical CV for a solution of $[Fe(CN)_6]^{3-/4-}$ in the presence of a gold working electrode before and after deposition of a mixed MUA:DT monolayer film is shown in Figure 2.7. On the bare gold electrode (dashed), the Faradaic current shows oxidation and reduction peaks with a separation of potential ΔE = 83 mV and a half-wave potential of $E_{1/2}$ = 225 mV *vs* Ag/AgCl. The current densities of oxidation and reduction reactions are identical, $j_{ox} = j_{red} = 277\ \mu A/cm^2$.

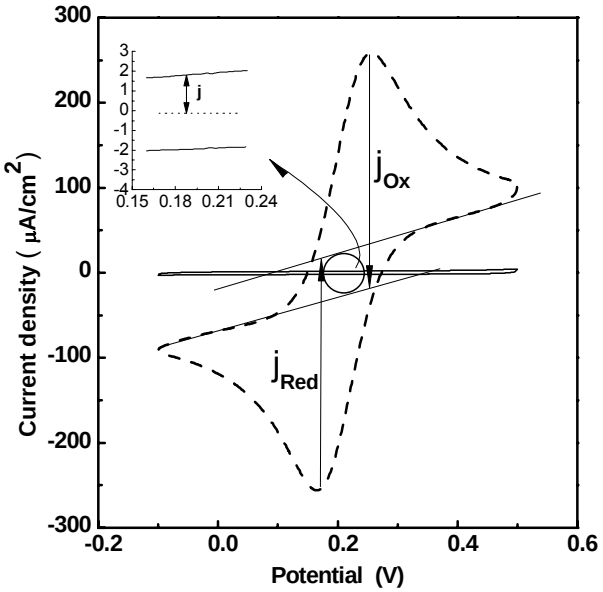

Figure 2.7: Cyclic voltammogram of a bare gold electrode (dashed) and a gold electrode modified with a mixed film of 11-mercaptoundecanonic acid (MUA) and 1-decanethiol (DT) in a 1:2 ratio (solid) in an equimolar solution of $[Fe(CN)_6]^{3-/4-}$ (1 mM), 0.5 M $NaClO_4$. Scan rate 0.1 V/sec, Ag/AgCl as reference and Pt wire as counter electrode. BAS gold electrode, 1.6 mm diameter).

However, in the presence of a typical mixed film prepared from a mixture of MUA and DT (solid), the film blocks the surface and keeps away the probe molecule from the surface. Therefore, no Faradaic current for the modified electrode is observed.

The CV obtained for the modified electrode shows that current density drops off to 2 $\mu A/cm^2$, which is around 0.7 % of the observed current density for a bare gold electrode. A typical blocking study for $[Boc\text{-}Gly\text{-}CSA]_2$ is shown in Figure 2.8. For this particular peptide conjugate, films exhibit a good blocking that reduced the Faradaic current to less than 1% of its original value, which is typical for well-packed films.

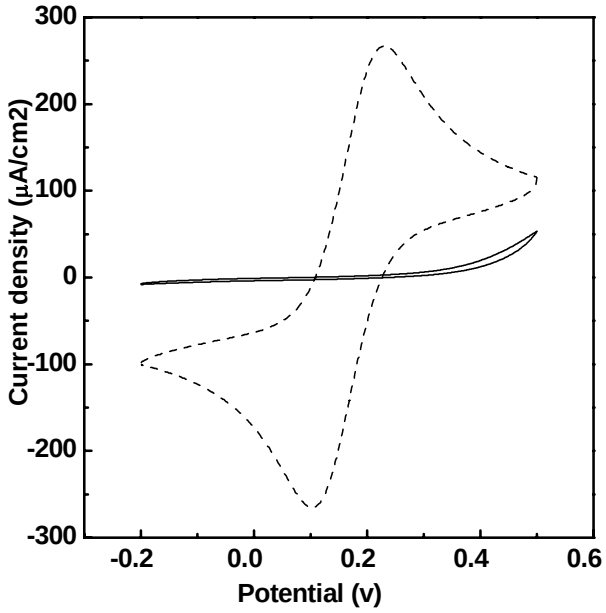

Figure 2.8: Cyclic voltammogram on a bare gold electrode (dash) and a gold electrode modified with Boc-Gly-CSA (solid) in an equimolar solution of $[Fe(CN)_6]^{3-/4-}$ (1 mM), 50 mM phosphate buffer. Scan rate 0.1 V/sec, Ag/AgCl as reference and Pt wire as counter electrode. BAS gold electrode, 1.6 mm diameter).

Self assembled monolayers of long chain alkanethiols provide stronger blocking than monolayers of peptide disulfides, presumably because of better arrangement of alkanethiol molecules.[27] Although the results obtained from CV method on peptide disulfide films showed an average charging current density of 3.5 $\mu A/cm^2$, which is comparable to that of obtained from MUA films, some amount of electro-activity in the

region of anodic potential leading to a maximum current density up to 25 $\mu A/cm^2$ were observed. This indicates that peptide disulfide films do not provide as efficient blocking as the thiolate films with a maximum current density up to 5.0 $\mu A/cm^2$. Moreover, impedance spectroscopy data demonstrate stronger blocking behavior for thiolate self assembled monolayers with a charge-transfer resistance ranging from 650 – 740 $K\Omega/cm^2$ (for example Figure 2.21), compared to the films containing peptide disulfide molecules with a charge-transfer resistance ranging from 150 to 200 $K\Omega/cm^2$ (such as Figure 2.15) . In conclusion, our results are consistent with the results of other works indicating alkanethiolates produce better formed monolayer than peptide disulfides. As a result, our studies indicate that MUA:DT films and the peptide disulfide films were well formed and have only a low amount of defects. Thus, they were used to investigate their behavior when exposed to nanoparticles (NPs).

Binary MUA/DT films on gold surfaces were characterized by non-electrochemical techniques such as reflection-absorption IR spectroscopy (RAIRS) and X-ray photoelectron spectroscopy (XPS). For this purpose, flat substrates were used, consisting of Au films on silicon. In this work, RAIRS and XPS measurements were obtained for the dilute MUA films.

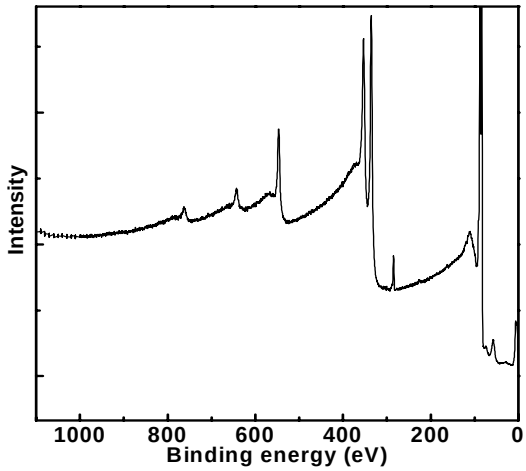

Figure 2.9: Survey spectra of a mixed film of 11-mercaptoundecanonic acid (MUA) and 1-decanethiol (DT) in a 1:5 ratio deposited onto Au surfaces.

The dilute MUA films of Au on Si were further examined by XPS. Initially, core level survey spectra were collected for the unmodified and binary film-modified gold substrates (Figure 2.9). To characterize the films present on the surfaces, high-resolution spectra were recorded for the main core level peaks of C, O, and S. High-resolution XPS spectra for the dilute MUA film are shown in Figure 2.10.

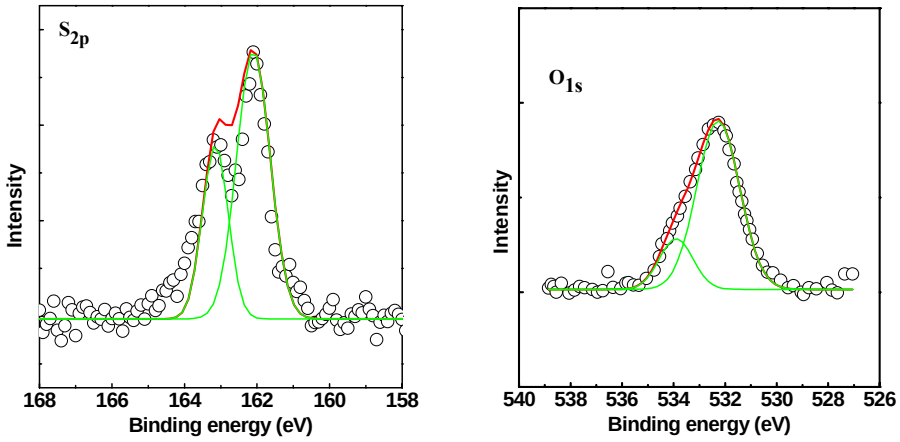

Figure 2.10: Core level XPS spectra of S2p and O1s of a mixed film of (MUA) and (DT) in a 1:5 ratio deposited onto Au surfaces.

Peaks in the region of 161.5-162.5 eV indicate Au-thiolate interactions due to the MUA on the gold surface.[33,59,60] We observed that the peak due to the thiolate occurred as a doublet at 161.9 and 163.3 eV for the $S_{2p3/2}$ and $S_{2p1/2}$ with a ratio of 2:1, which supported the formation of a gold-sulfur bond.[61] The O_{1s} spectrum was deconvoluted into two peaks; at 533.9 eV due to the double-bonded (C=O) and at 532.2 eV due to the single bonded oxygen (OH/C-O).

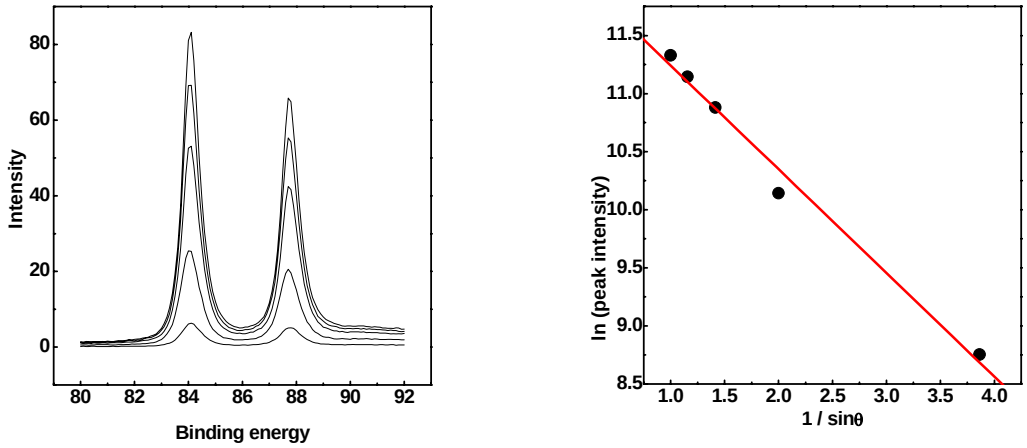

Figure 2.11: ARXPS measurements for the Au_{4f} (left), and the graph of 1/sinθ and ln of the peak intensities of $Au_{4f7/2}$ for a mixed films of (MUA) and (DT) in 1:5 ratio on a flat gold substrate (right). Au (200 μm on Si, Platypus Technologies, Inc.)

Angle-resolved XPS (ARXPS) measurements were used to determine the thickness of the dilute MUA film from the attenuation of the Au_{4f} signals of the gold substrate. The photoelectron intensity from the thin film-covered substrate varies with the take off angle, θ (taken as the angle between the surface plane and entrance to the analyzer), and is given by equation **1:**[62,63]

$$\ln(I) = -d/(\lambda \sin\theta) + \ln(I_0) \qquad (\mathbf{1})$$

where I_0 and I are the intensities of the photoelectron from the clean substrate and from the covered substrates, respectively. Value d is the film thickness and λ is the inelastic

mean free paths of photoelectrons. Accordingly, ln(I) should be linearly related to 1/sinθ with a slope of -d/λ. Thus, the ratio -d/λ allows for an evaluation of the film thickness. Figure 2.11 shows a typical ARXPS for Au_{4f} core levels for a mixed film of 11-mercaptoundecanonic acid (MUA) and 1-decanethiol (DT) in 1:5 ratio, measured at various θ angles and the related plot of ln(I) versus 1/sinθ graph for the two Au_{4f} signals. The two peaks due to $Au_{4f5/2}$ and $Au_{4f7/2}$ were observed at 87.8 and 84.2 eV, respectively.[30,33] The intensities of these peaks decreased with the decrease in θ and plots of ln(I) verses 1/sinθ were linear for DT-diluted MUA films, at higher sampling angles. The slope of -d/λ, derived from the linear section of the ln(I) *vs* 1/sinθ plot for the $Au_{4f7/2}$ at 84.2 eV, was calculated to be -0.89. An experimental film thickness d = 37.4 (5) Å was obtained from the plot, assuming a λ value of 42 Å.[30] This is clearly too thick for a film of MUA. Experimental film thickness reported by other groups for MUA films are in the range of 12-18 Å.[27,64] Molecular Mechanics Force Field (MMFF) optimization using SPARTAN (Irvine, CA) of a molecule of 11-undecanoic acid provides an estimate of the film thickness of 16.1 Å, which is consistent with experimental results obtained by other groups. (Table 2.2)

Table 2.2: Comparison between Experimental and Theoretical Film Thickness from ARXPS Measurements for dilute MUA film on gold substrates

Film	Slope (-d/λ)	Experimental thickness (Å)	Theoretical thickness (Å)	Reference
MUA:DT (1:5)	-0.89	37.4	16.1	This work
MUA	-1.1	37	16	Reference [27]
MUA		12-18		Reference [64]

The differences between the observed 37.4 Å and the theoretical 16.1 Å thicknesses for MUA might be due to the formation of dimers, which has been confirmed by the IR stretching vibrations at 1710 cm^{-1} (Figure 2.13) and was reported before by David L. Allara and coworkers.[24,65]

Reflection-absorption infra-red spectroscopy (RAIRS) measurements were initially used to characterize the dilute MUA film on gold substrate and then to investigate the interactions between the film and Gly-CSA-Au NPs. In the beginning, RAIRS were recorded for a mixed film of 11-mercaptoundecanonic acid (MUA) and 1-decanethiol (DT) in a 1:2 ratio on gold.

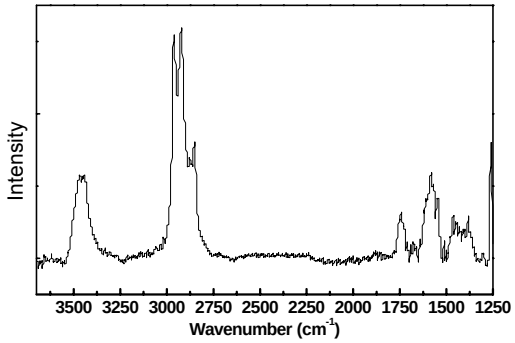

Figure 2.12: RAIR spectra of a mixed film of 11-mercaptoundecanonic acid (MUA) and 1-decanethiol (DT) in 1:2 ratio on a gold substrate

Figure 2.12 shows the RAIR spectrum for a DT-diluted MUA film on a Au substrate. A number of selected absorbance bands and their spectral assignments are listed in Table 2.3. The spectra of these surfaces are characterized by a strong absorbance in the 3000-2800 cm^{-1} region as result of C-H stretching vibrations of methylene and methyl groups. The strong absorbance at 2960 cm^{-1} is attributed to the asymmetric stretching mode $\upsilon_{C\text{-}H}$ of the methyl group of the decanethiol. The two absorbance bands at 2920 and 2850

cm^{-1} are assigned to the asymmetric stretching mode υ_{C-H} of methylene groups of both MUA and decanethiol.[24,66]

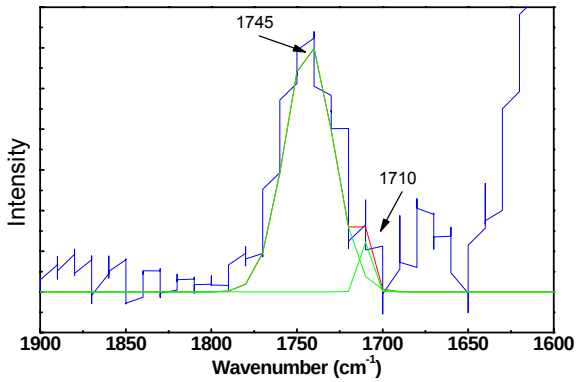

Figure 2.13: The two absorbance bands for C=O stretching of non-hydrogen-bonded and hydrogen-bonded carboxylic acid functional groups.

An intense absorbance at 1745 cm^{-1} is due to the $\upsilon_{C=O}$ stretching of non-hydrogen-boned carboxylic group and a very weak band at 1710 cm^{-1} is resulted from the stretching $\upsilon_{C=O}$ of hydrogen-bond carboxylic group[67], indicating there are some face to face hydrogen bonds between two MUA molecules.[24,68,69]

Table 2.3: RAIR Spectral mode assignments for the diluted MUA film on gold surface

Wavenumber (cm^{-1})	Mode assignment
2960	CH_3 C-H str (asym)
2920	CH_2 C-H str (asym)
2850	CH_2 C-H str (sym)
1745	non-hydrogen-bonded C=O str
1710	hydrogen-bonded C=O str
1440-1460	CH_2 scissors def
1300	C-O str

Despite the presence of H-bonded dimers, a comparison of the intensities of the bands of the free acid and the H-bonded dimers shows that most of the MUA molecules are present on the surface as free acid molecules and will be able to interact with gold NPs (see Figure 2.13). Two absorbance bands observed at 1440 and 1460 cm^{-1} are attributed to scissor deformation modes, δ_{C-H} of the CH_2 groups, including those in the α position to C=O. The band at 1300 cm^{-1} is attributed to the υ_{C-O} of the acid group.[70]

2.3. The Interaction of Films with Gold Nanoparticles

This section describes the interactions between the modified gold surfaces described earlier and gold nanoparticles (NPs). Three films were investigated having neutral, charged, hydrogen bond donor-acceptor groups facing the solution, and the interactions with NPs were studied using a variety of methods. For this study, we made use of two types of water soluble NPs. The first group of NPs was coated with MUA giving MUA-Au NPs, which possess a carboxylic acid group. The second group of NPs was modified by Gly-CSA giving Gly-CSA-Au NPs, which possess a free amine group. Both groups of NPs were synthesized with an average diameter of around 4.5 nm by Mita Dasog in Dr. Scott's research group (University of Saskatchewan).

The peptide disulfides described in Chapter 2.1 were used to prepare a range of films that possess different surface characteristics. In the following chapters, the results obtained by exploring the systems will be explained and discussed.

2.3.1. System of Neutral Films

The objective was to investigate the possible interactions of NPs with neutral peptide molecules linked to a gold surface. The study begins with the investigation of neutral films prepared from Boc-protected peptide disulfide compounds **1** and **2**. As described in Section 2.2, these films are well packed and show good blocking behavior towards the anionic $[Fe(CN)_6]^{3-/4-}$ redox probe. Figure 2.14 shows the CV of the anionic $[Fe(CN)_6]^{3-/4-}$ redox probe on a gold electrode modified with films prepared from [Boc-Gly-CSA]$_2$ (**1**) before and after the addition of MUA-coated gold NPs. The film before exposure to NPs shows a small amount of charge transfer at the high anodic side of the potential window. However, after exposure to the NPs the maximum current density dropped from 25.5 $\mu A/cm^2$, to 15.4 $\mu A/cm^2$, indicating that the NPs enhance the blocking of the surface towards the anionic redox probe. This suggests that the NPs interact with the surface under these conditions. At pH 7, the MUA films will be deprotonated. The resulting carboxylates will electrostatically repel the anionic $[Fe(CN)_6]^{3-/4-}$ redox probe from the surface, leading to a lower observed current density in the presence of the NPs.

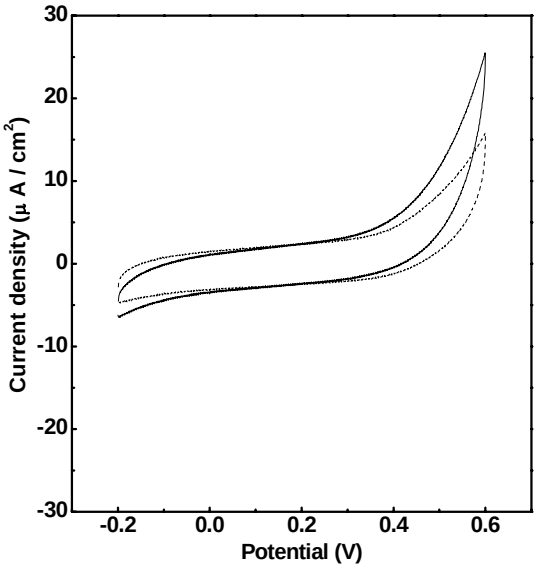

Figure 2.14: CV of $[Fe(CN)_6]^{3-/4-}$ (1 mM) at a gold electrode (BAS, 1.6 mm) modified with a film prepared from $[Boc\text{-}Gly\text{-}CSA]_2$ (**1**) before (solid) and after (dashed) exposure to MUA-Au NPs (dashed) in 50 mM phosphate buffer at pH = 7

The results of an electrochemical impedance spectroscopy (EIS) study of the film of $[Boc\text{-}Gly\text{-}CSA]_2$ (**1**) on gold electrodes before and after the addition of MUA-modified nanoparticles is shown in the Nyquist plot in Figure 2.15. The impedance data is fitted to a modified Randel circuit, which possesses a constant phase element (CPE) instead of a capacitor, allowing interpretation with the help of circuit elements (see Table 2.3). For a film of compound **1** on gold electrodes (BAS, diameter 1.6 mm), the charge transfer resistance of about 217 kΩ together with the CV results indicate a well-packed monolayer on the electrode surface. However, the equivalent circuit consists of a CPE element with n = 0.93 which indicates that the double layer capacitor is not an ideal capacitor element. This accounts for some of the heterogeneity in the make-up of the film.

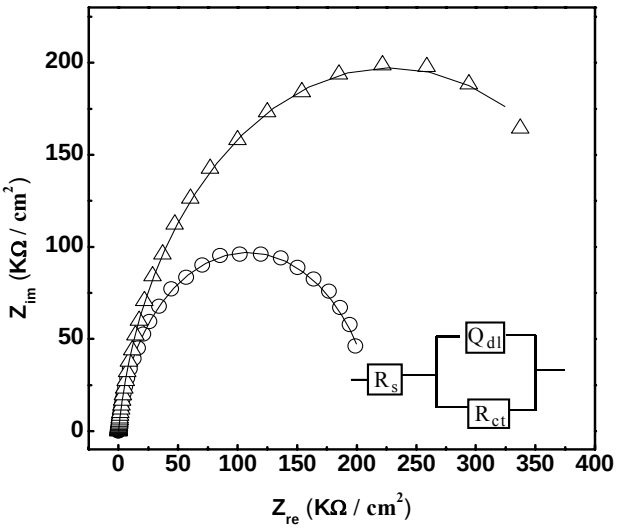

Figure 2.15: Nyquist plots showing impedance behavior of films prepared from [Boc-Gly-CSA]$_2$ (**1**) on gold electrodes before (○) and after (**Δ**) exposure of the film to MUA-Au NPs. The EIS was recorded at the $E_{1/2}$ of the $[Fe(CN)_6]^{3-/4-}$ redox couple (E = 0.17 V). The frequency range was from 100 kHz to 0.01 Hz, and the modulation amplitude was 5 mV rms. The continuous lines correspond to fits of a classic Randle's equivalent circuit.

After the addition of the MUA-modified NPs, the charge transfer resistance R_{CT} more than doubled to 456 KΩ. This is a significant change, which is rationalized with the help of a cartoon shown in Scheme 2.5. The NPs are coated with MUA which is a carboxylic acid terminated ligand and at pH = 7, when most of them are expected to be deprotonated.[71-73]

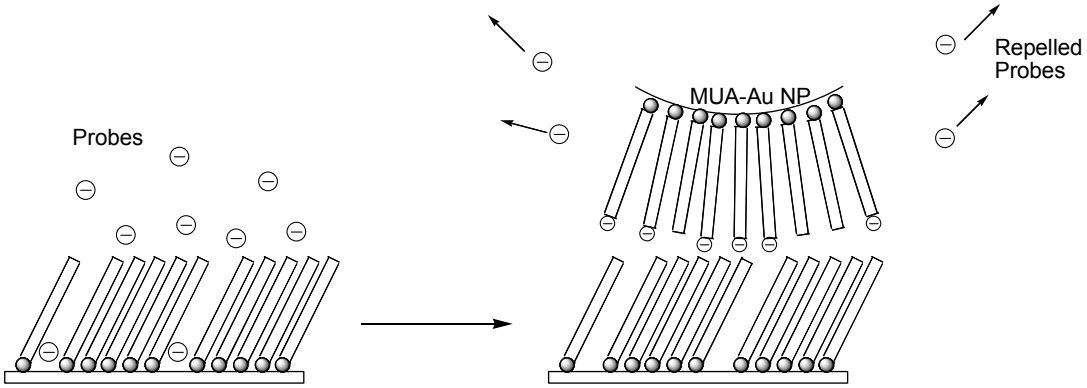

Scheme 2.5: Schematic representation of the behavior of a film of [Boc-Gly-CSA]$_2$ (**1**)

exposed to MUA-Au NPs at pH = 7

The peptide disulfide film was immersed in a solution of NPs with a pH adjusted to 7 using a phosphate buffer for 30 – 60 min. Adjusting the pH does not change the surface charge of the peptide film on the electrode surface, but it affects the MUA-modified NPs and is expected that the NPs are negatively charged at this pH. In the absence of the NPs, the anionic redox probe $[Fe(CN)_6]^{3-/4-}$ may penetrate the peptide film, particularly in places with pinholes, giving rise to the observed CVs and a decline in charge transfer resistance.

Table 2.4: The circuit elements for the electrochemical reactivity of $[Fe(CN)_6]^{3-/4-}$ at films of $[Boc\text{-}Gly\text{-}CSA]_2$ (**1**) in the presence and absence of MUA-Au NPs

	Compound **1** No MUA-modified Au NPs	Compound **1** MUA-Au NPs added
Q_{dl} (S-sec$^{1/2}$/cm^2)	12.6 (3)	13.8 (3)
n	0.93 (0.05)	0.91 (0.05)
R_{ct} (KΩ/cm^2)	217 (50)	456 (50)

However, the anionic NPs added to the system interact with the peptide surface, resulting in the repulsion between the negatively charged $[Fe(CN)_6]^{3-/4-}$ and negatively charged MUA-modified NPs. This in turn will result in a reduced charge density and an increased charge transfer resistance, as was observed experimentally. This suggests that the NPs may interact with the surfaces specifically, presumably by H-bonding of the MUA carboxylates on the NPs with the peptide NHs present in the peptide film.

Figure 2.16 shows a film of $[Boc\text{-}Asp(Bz)\text{-}CSA]_2$ (**2**) on a gold electrode surface before and after exposure to MUA-Au NPs. The film shows the same behavior as a film of $[Boc\text{-}Gly\text{-}CSA]_2$ when exposed to MUA-coated gold NPs. A small decline in maximum current density is observed in the CV of $[Fe(CN)_6]^{3-/4-}$ for this system.

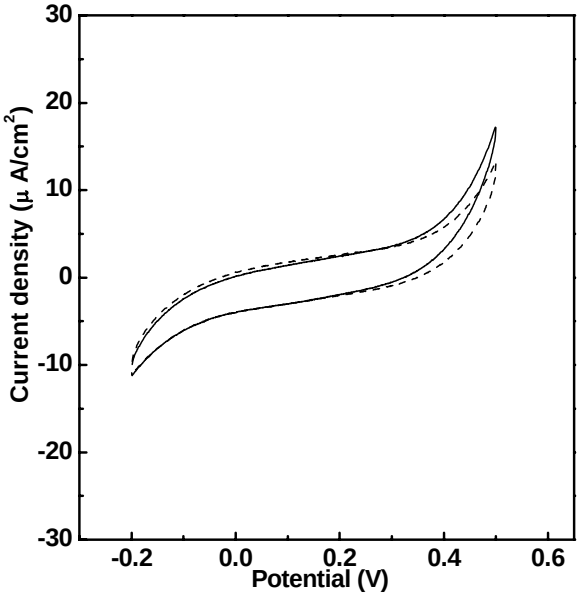

Figure 2.16: CV of $[Fe(CN)_6]^{3-/4-}$ (1mM) at a film prepared from $[Boc\text{-}Asp(Bz)\text{-}CSA]_2$ (**2**) on gold electrode before (solid) and after exposure to MUA-Au NPs (dashed) in 50 mM phosphate buffer at pH = 7.

The interaction with MUA-Au NPs gives similar results to those of Boc-Gly-CSA films, also indicating an interaction of the MUA-modified NPs with the peptide surface. A typical Nyquist plot obtained for $[Fe(CN)_6]^{3-/4-}$ at a film of compound **2** before and after treating it with MUA-Au NPs is shown in Figure 2.17. The continuous lines correspond to the fit of the data to a modified Randel equivalent circuit, from which average charge-transfer resistances of 175 and 229 KΩ were obtained for the this system before and after the interaction with MUA-Au NPs, respectively. This indicates that the behavior of the Boc-Asp(Bz)-CSA films were affected by the NPs similarly as Boc-Gly-CSA films.

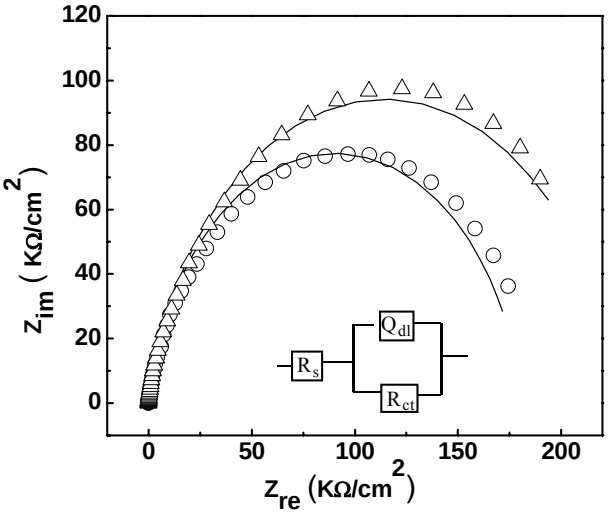

Figure 2.17: Nyquist plots showing impedance behavior of $[Fe(CN)_6]^{3-/4-}$ at a film of [Boc-Asp(Bz)-CSA]$_2$ (**2**) on gold electrode before (○)**,** and after (**Δ**) exposure to MUA-Au NPs (**Δ**). The EIS was recorded at the $E_{1/2}$ of the $[Fe(CN)_6]^{3-/4-}$ redox couple (E = 0.17 V). The frequency range was from 100 kHz to 0.01 Hz, and the modulation amplitude was 5 mV rms. The continuous lines correspond to fits of a classic Randle's equivalent circuit.

Next, we proceeded to test our hypothesis of the interaction between the NPs and the surface. If our assumption is correct, we can expect an opposite tendency in the CV and EIS for the interaction of NPs coated with cationic terminated ligands. Thus, we proceeded to perform similar experiments with gold NPs modified with Gly-CSA. The capping ligand possesses a free amine. However, at pH = 7, is expected that the amine group is protonated and positively charged.[74-76] The system consisting of a film of compound **2** and Gly-CSA-modified Au NPs in the presence of $[Fe(CN)_6]^{3-/4-}$ as an anionic probe has been schematically illustrated in Scheme 2.6.

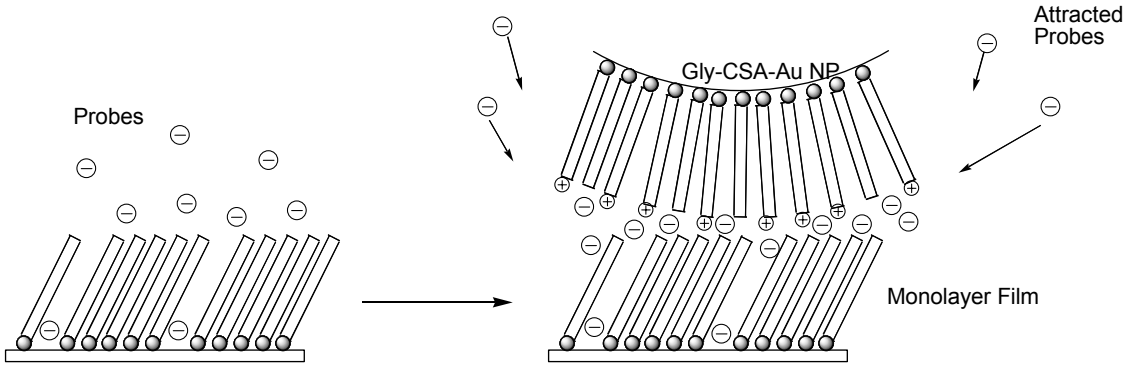

Scheme 2.6: Schematic representation for the behavior of a film of [Boc-Asp(Bz)-CSA]$_2$ exposed to Gly-CSA-modified Au NPs at pH = 7

The above cartoon illustrates that positively charged NPs could facilitate the communication between the anionic probes and the modified electrode surface through electrostatic attractions. This will enhance the electrochemical activity and thus, the charge transfer resistance is expected to decrease. The results of our electrochemical study of this system are shown in Figures 2.18 and 2.19 and are in agreement with our prediction.

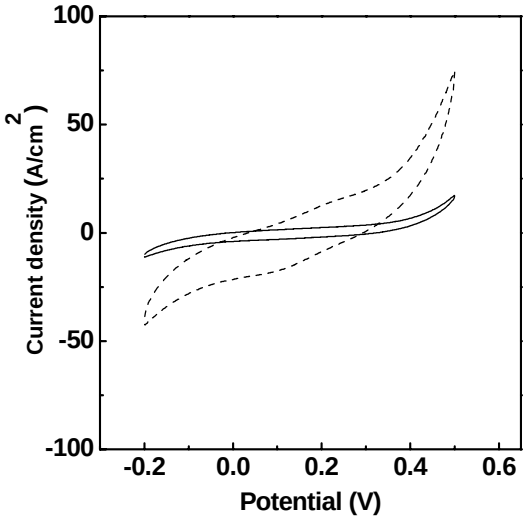

Figure 2.18: CV of $[Fe(CN)_6]^{3-/4-}$ at film of [Boc-Asp(Bz)-CSA]$_2$ (**2**) on a gold electrode before (solid) and after exposure to Gly-CSA-modified Au NPs (dashed) in 50 mM phosphate buffer at pH = 7.

The apparent increment of the current density along with the decrease in the charge transfer resistance induced by the NPs can be rationalized in terms of (i) an increase in interfacial concentration of the anionic redox species due to a strong affinity to the polycationic NPs and/or (ii) by an increase in defects of the self-assembled film exposing active sites at the electrode surface. However, our results obtained from the system of hydrogen bond donor-acceptor films indicate that the latter is not significant. (see Section 2.3.3)

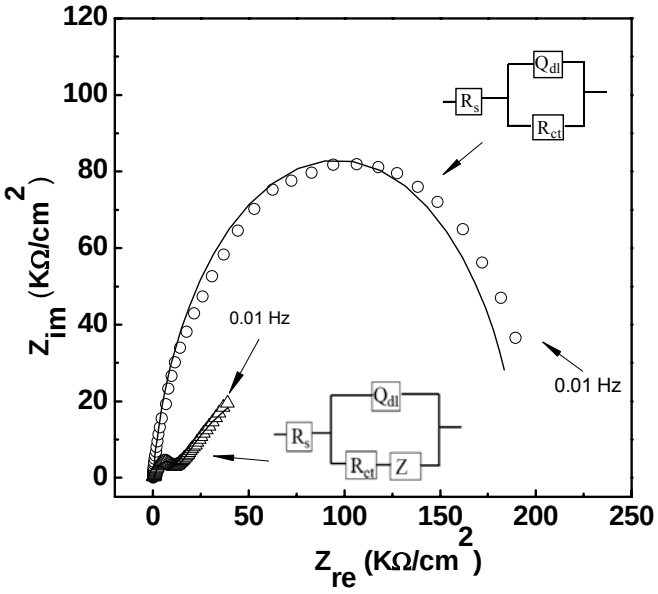

Figure 2.19: Nyquist plots showing impedance behavior of $[Fe(CN)_6]^{3-/4-}$ at a film of **[**Boc-Asp(Bz)-CSA]$_2$ on gold electrode before (○) and after (**Δ**) exposure to Gly-CSA-Au NPs. The EIS was recorded at the $E_{1/2}$ of the $[Fe(CN)_6]^{3-/4-}$ redox couple (E = 0.17 V). The frequency range was from 100 kHz to 0.01 Hz, and the modulation amplitude was 5 mV rms. The continuous lines correspond to fits of classic and modified Randle's equivalent circuits.

2.3.2. System of Charged Films

To study the behavior of charged films exposed to NPs, Gly-CSA and DT-diluted MUA films were studied. Both films have ionizable groups, and the experimental conditions are adjusted to keep the Gly-CSA film cationic and the MUA film anionic. In this section, the experimental results of the interactions of the cationic Gly-CSA film with anionic MUA-modified Au NPs and of the anionic DT-diluted MUA film with cationic Gly-CSA-modified Au NPs, will be presented and discussed.

2.3.2.1. The Interaction of MUA Film with Gly-CSA-modified Gold Nanoparticles

Films of DT-diluted MUA were prepared by self-assembly from a binary 1 mM solution of MUA and DT in a ratio of 1:2, as described in Chapter 2.2.2. The rationale for using diluted MUA films was to avoid lateral H-bonding interactions between the carboxylic acids of MUA. Essentially, dilution will space apart the MUA molecules as illustrated previously in Figure 2.6. Other studies have shown this to be an effective method for preventing such lateral interactions, which may interfere with the interaction of the MUA films with the modified Au NPs.[52]

Since longer chain alkanethiols generate very well packed and organized monolayers on gold surfaces,[27] we do not observe any Faradaic signal due to the $[Fe(CN)_6]^{3-/4-}$ redox probe in solution, indicating a well-blocked surface. The CVs of the $[Fe(CN)_6]^{3-/4-}$ redox probe at a DT-diluted MUA film before and after exposure to Gly-CSA-modified Au NPs is shown in Figure 2.20.

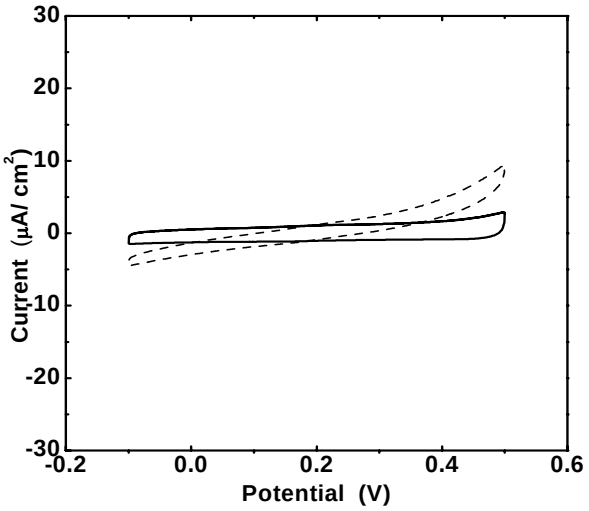

Figure2.20: CV of $[Fe(CN)_6]^{3-/4-}$ (1mM) at a DT-diluted MUA film on gold electrode before (solid) and after exposure to Gly-CSA-modified Au NPs (dashed) in 50 mM phosphate buffer at pH = 7. Ag/AgCl reference electrode, Pt counter electrode, scan rate = 100 mVs^{-1}

The DT-diluted MUA film insulates and protects the electrode surface from the electro-active probe present in solution. As a result, the CV lacks a Faradaic signal and exhibits only charging current due to charging of the double layer[37,55] with a maximum current density of 2.8 $\mu A/cm^2$. This current density compared with that of a bare gold, 250.7 $\mu A/cm^2$ shows that this film effectively blocks the surface.

The increase in current density (Figure 2.20) indicates more electrochemical reactivity on the surface when the DT-diluted film is exposed to Gly-CSA-modified Au NPs. This is consistent with our result for the neutral films exposed to the same cationic NPs. On the other hand, the charge-transfer resistance R_{CT}, obtained from a fit of the impedance data to a Randles equivalent circuit (Figure 2.21), significantly decreases in the presence of the cationic NPs from 736.5 KΩ for the film before exposure to 97.3 KΩ after exposure to the NPs.

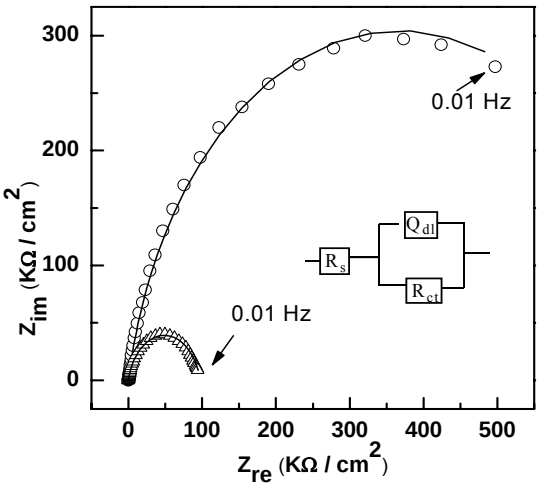

Figure 2.21: Nyquist plots showing impedance behavior of DT-diluted MUA films on gold electrodes (○) before and (**Δ**) after exposure to Gly-CSA-Au NPs. The EIS was recorded at the $E_{1/2}$ of the $[Fe(CN)_6]^{3-/4-}$ redox couple (E = 0.17 V). The frequency was in the range of 100 kHz to 0.01 Hz, and the ac modulation amplitude was 5 mV. The continuous lines correspond to fits of a modified Randle's equivalent circuit.

Scheme 2.7 illustrates the potential electrostatic interaction between the negatively charged DT-diluted MUA film with the cationic Gly-CSA-modified Au NPs. In the absence of the cationic NPs, the anionic $[Fc(CN)_6]^{3-/4-}$ redox probes is electrostatically repelled from the surface, leading to a lack of Faradaic current in the CV and a high R_{CT}.

However, in the presence of cationic NPs, electrostatic interactions will attract the anionic $[Fc(CN)_6]^{3-/4-}$ redox probes to the NPs, which will be brought in close contact with the film surface. In addition, the electrostatic interactions between the NPs and the film may also disturb the film and may help the redox probes to penetrate the film, resulting in the observed Faradaic signal and a significantly lower R_{CT} for the latter case.

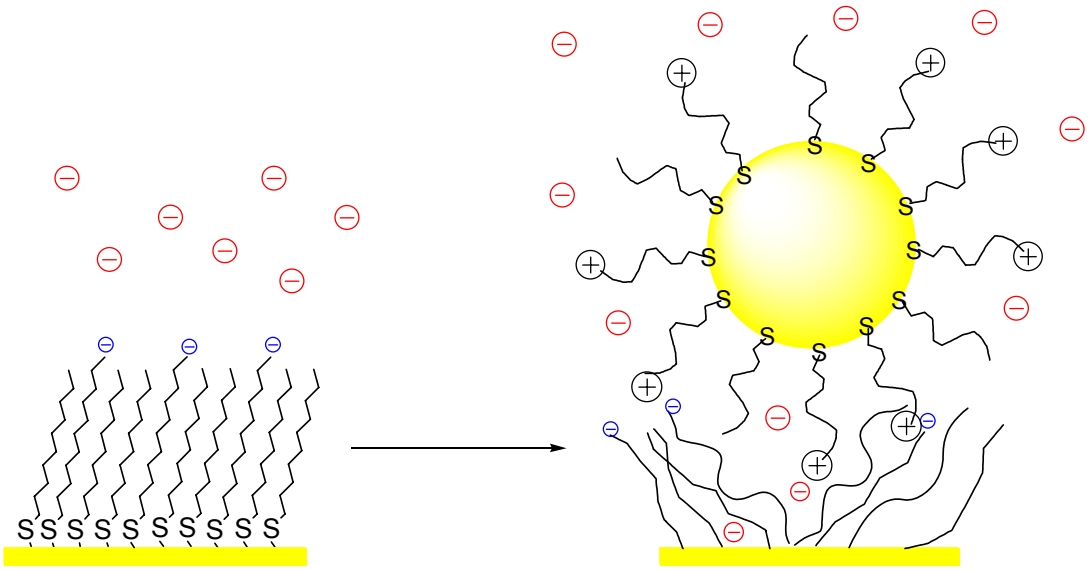

Scheme 2.7: Schematic representation of the interactions between an anionic film and cationic NPs in presence of anionic redox probes

In order to get more insight into the interactions that takes place on this surface, RAIRS experiments were carried out. As was discussed in section 2.2.3, RAIRS was used to characterize DT-diluted MUA films on Au surfaces. The FT-RAIR spectrum of a DT-diluted MUA-modified gold surface before and after exposure to Gly-CSA-modified Au NPs is shown in Figure 2.22. The modified NPs have an amide moiety, which can serve as a fingerprint for the presence of the NPs on the surface. The broad band in the region of 3380-3160 cm^{-1} can be related to the NH stretching vibration of the peptide amide.

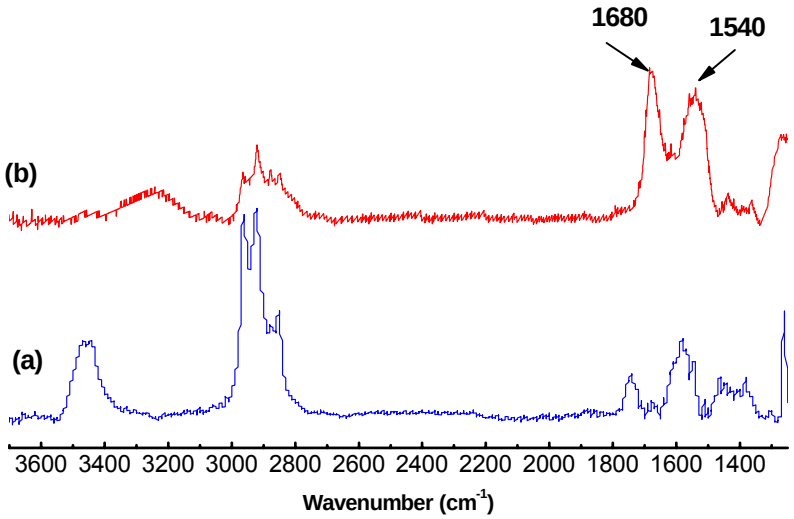

Figure 2.22: FT-RAIR spectrum of DT-diluted MUA film on a gold substrate (a) before and after exposure to Gly-CSA-Au NPs

Although the spectra does not have a good resolution, we may be able to assign some characteristic bands, which can confirm our interpretation about the presence of NPs on the film surface. The band at 1684 cm^{-1} is assigned to $\upsilon_{C=O}$ stretching mode and 1542 cm^{-1} to υ_{C-N} stretching and δ_{N-H} bending modes of amide, which support the presence of the NPs attracted by the MUA film (Table 2.5).[66,70,77-79]

Table 2.5: Selected RAIR Spectral mode assignments for the diluted MUA film on gold surface exposed to Gly-CSA-Au NPs

Wavenumber (cm^{-1})	Mode assignment
3380-3160	N-H str
2920	CH_2 C-H str (asym)
2850	CH_2 C-H str (sym)
1684	C=O amide str
1540	amide (C-N) str and (N-H) bending

To gain more insight into the NP adsorption on the DT-diluted MUA film, quartz crystal microbalance experiments (QCM) were carried out, which allow determination of mass changes that take place upon the adsorption of Gly-CSA-modified Au NPs on the DT-dilute MUA film. The preparation of the DT-diluted MUA film on gold covered silicon crystals (9 mm diameter, AT-cut, CH Instruments) was identical to that described for the preparation of the other surfaces. Changes in the resonance frequency Δf were monitored as a function of time (in s).

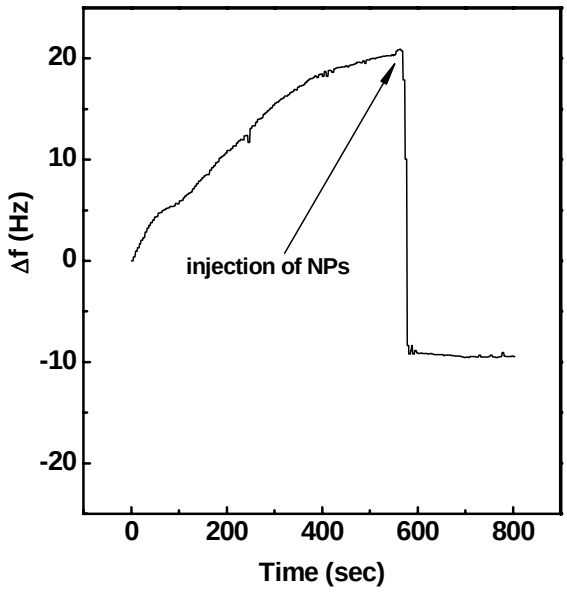

Figure 2.22: Typical QCM plot showing the changes in frequency (Δf) as a function of Time (s) of a DT-diluted MUA modified Au surfaces on a quartz crystal. Gly-CSA-modified Au NPs were introduced to the system at 566 s. T = 23 °C.

Figure 2.22 shows a plot of the change in resonance frequency Δf in Hz versus time in seconds. A solution of Gly-CSA-modified Au NPs (200 µl, 50 mg/L) was added and the changes in Δf were monitored. The addition of the NPs solution resulted in a decrease in the frequency of 30.3 (± 5) Hz, which corresponds to a net mass increase of

43.2 ng. The same experiment was carried out under identical conditions on bare Au as a control experiment and a net mass gain of 12.5 ng was observed after addition of the NPs. This suggests that some NPs adsorb onto the surface. However, the mass gain in the presence of the DT-diluted MUA film is significantly larger, which is consistent with the model suggesting an interaction between the surface and the NPs.

The mass of NPs adsorbed on the film due to the attractions between the two is calculated as the difference between the mass changes in the control and the film experiment, giving a mass change of 30.6 ng. The theoretical mass change is calculated by using the average molar mass of NPs (5.59×10^5 g/mol), an average footprint of 1.96×10^{-13} cm^2, and the known crystal surface area of 0.205 cm^2, giving a theoretical mass increase for 100% monolayer of the crystal surface of 970.3 ng. This indicates that only a small amount of the surface is actually covered with NPs (ca. 3.1%). This low amount of adsorption of the NPs can be rationalized by considering the electrostatic repulsion between the cationic NPs.

Table 2.6. Frequency and mass changes on QCM after deposition of dilute MUA film and exposure to NPs

Gly-CSA-Au NPs added onto Surfaces of	Frequency change(Δf) Hz	Mass change (Δm) ng	Calc. mass changes (ng)
Bare gold	8.8	12.6	-
MUA:DT	30.3	43.2(±)	-
Net adsorbed	21.5	30.6	970.3

2.3.2.2. The Interaction of Gly-CSA Films with MUA-modified Gold Nanoparticles

A cationic film could be expected to show the opposite behavior when it is exposed to anionic NPs in a presence of an anionic redox probe. Figure 2.23 shows the effect of Boc-deprotection on the signal of the $[Fe(CN)_6]^{3-/4-}$. The film of Boc-Gly-CSA exhibits good blocking behavior (Figure 2.23 a). However, upon Boc-deprotection with trifluoroacetic acid (TFA), the surface is cationic, having ammonium groups facing the solution. The amine group on Glycine has a pK_a of 9.6 in solution, based on literature, is expected to have a pK_a around 7.5, which indicates at least 50% of the amine groups are protonated at pH = 7.[74-76] Expectedly, the CV shows an increase in the current density, presumably due to an increase in the interfacial concentration of the anionic redox probes at electrode surface through electrostatic attractions.

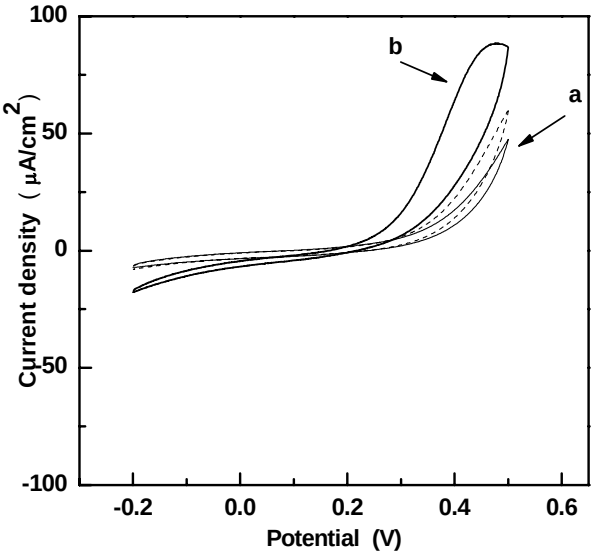

Figure 2.23: CV of $[Fe(CN)_6]^{3-/4-}$ (1mM) at a film of $[Boc\text{-}Gly\text{-}CSA]_2$ (**1**) on a gold electrode (BAS, 1.6 mm diameter) a) before and b) after Boc-deprotection. After deprotection, the film is exposed to MUA-modified Au NPs (dashed). 50 mM phosphate buffer, pH = 7, Ag/AgCl reference electrode, Pt counter electrode, scan rate = 100 mV/s

At this point it cannot be ruled out that Boc-deprotection with TFA might result in some loss of thiolate from the surface.[52,80] However, exposing the cationic film to the anionic NPs led to an obvious decrease in current density. We observed this behavior before for the neutral film system. A decrease in current density indicates a higher charge-transfer resistance. Figure 2.24 shows a typical Nyquist plot of the cationic Gly-CSA film and the modified Randles' circuit used to interpret the EIS data. From the EIS it is apparent that there is an increase in R_{CT} upon interaction of the anionic NPs with the cationic film. The presence of anionic NPs will enhance the surface blocking with respect to the anionic $[Fe(CN)_6]^{3-/4-}$ redox probes due to the electrostatic repulsion between the anionic probes and anionic NPs.

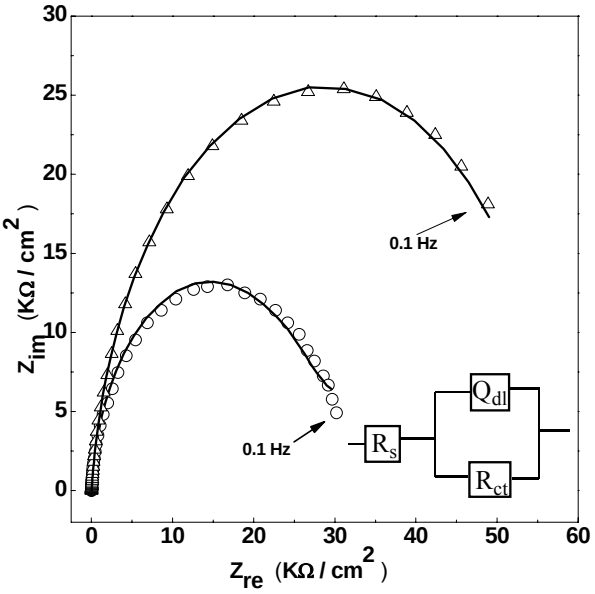

Figure 2.24: Nyquist plots showing impedance behavior of films of compound **1** after Boc-deprotection (○) and after exposure to MUA–modified Au NPs (**Δ**). The EIS was recorded at the $E_{1/2}$ of the $[Fe(CN)_6]^{3-/4-}$ redox couple (E = 0.17 V). The frequency range was from 100 kHz to 0.01 Hz, and the ac modulation amplitude was 5 mV. The continuous lines correspond to fits of a classic Randle's equivalent circuit.

2.3.3. System of hydrogen bond donor-acceptor Films

The role of hydrogen-bonding interactions was investigated by using gold surfaces and Au NPs, both modified with MUA. In acidic media (pH < 4),[71-73] the carboxyl groups of MUA remain protonated and are able to interact via hydrogen-bonding interactions.[33] Figure 2.25 shows an approximately 30% increase in R_{CT}, when a dilute MUA- modified electrode was exposed to MUA-Au NPs in acidic pH, which gives a strong indication of the presence of attracted NPs on the film due to the hydrogen bond interactions.

Scheme 2.8 illustrates the behavior of the dilute MUA films as a function of pH and NP addition. At a pH 7, the carboxylic acid groups of DT-diluted MUA film will be deprotonated, resulting in a strong electrostatic repulsion of the anionic $[Fe(CN)_6]^{3-/4-}$ from the surface. Charge transfer resistance for the anionic film was measured to be 360.4 KΩ/cm^2 (Figure 2.25).

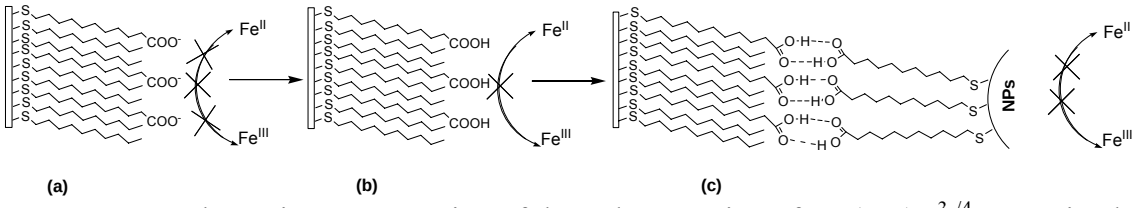

Scheme 2.9: Schematic representation of the redox reaction of $[Fe(CN)_6]^{3-/4-}$ at a mixed MUA/DT film on gold. (a) pH = 7 - strong electrostatic repulsion; (b) pH = 3 – some blocking due to a well-packed surface; (c) the film exposed to MUA-modified Au NPs at pH = 3.

At pH = 3, the film is fully protonated and the R_{CT} is decreased to 22.5 KΩ/cm^2. In the presence of the NPs, the system is slightly more compact and provides an increased blockage, resulting in a slight increase in R_{CT} to 29.5 KΩ/cm^2.

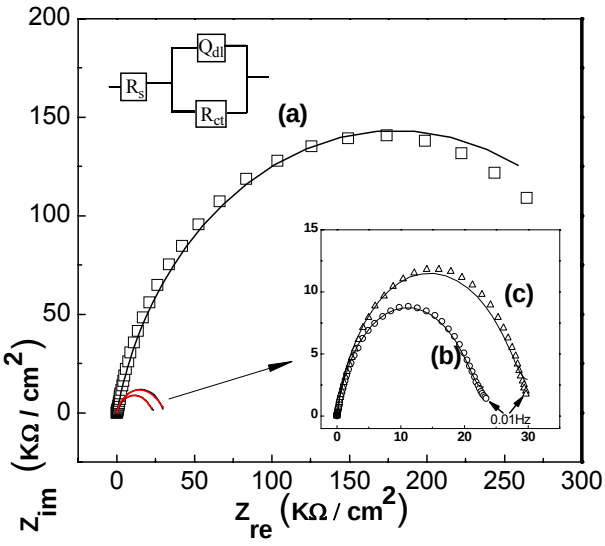

Figure 2.25: Nyquist plots showing impedance behavior of a DT-diluted MUA film on a gold electrode at (a) pH = 7, (b) at pH = 3, and (c) in the presence of MUA–modified Au NPs at pH = 3. The EIS was recorded at the $E_{1/2}$ of the $[Fe(CN)_6]^{3-/4-}$ redox couple (E = 0.17 V). The frequency was in the range of 100 kHz to 0.01 Hz, and the ac modulation amplitude was 5 mV. The continuous lines correspond to fits of a classic Randle's equivalent circuit.

The significant effect of acidic pH on R_{CT} raises the question: if the acidic media damages the film, resulting in the decrease of R_{CT}, is it due to a less tightly packed film or a large amount of the defects created among the film by the acid treatment? In order to address this question, a control impedance experiment was carried out on the MUA-modified Au electrode at different pH. The behavior of the monolayer was monitored when the pH of the solution was being changed. The Nyquist plot of the monolayer initially at pH = 7 showed a large charge transfer resistance, whereas it was dramatically decreased at pH = 3. However, by increasing the pH back to its initial value (pH = 7), the monolayer showed the same behavior as it had at the beginning (Figure 2.26). This resulted in a complete recovery of R_{CT} to the level of a deprotonated carboxylate film, indicating that the acid treatment did not damage the film.

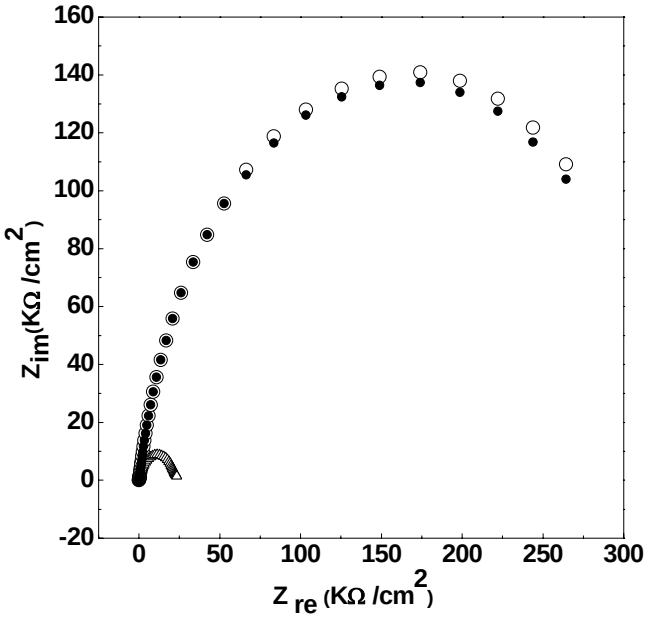

Figure 2.26: Nyquist plots showing impedance behavior of a DT-diluted MUA film on a gold electrode at (○) pH = 7, (**Δ**) at pH = 3, and (●) at pH recovered back to 7. The EIS was recorded at the $E_{1/2}$ of the $[Fe(CN)_6]^{3-/4-}$ redox couple (E = 0.17 V). The frequency was in the range of 100 kHz to 0.01 Hz, and the ac modulation amplitude was 5 mV.

3. CONCLUSION AND FUTURE WORK

The objective of this project was to study the interaction of water-soluble Au nanoparticles with biomolecules. I decided to approach this problem using a surface-based approach. Chemically modified Au NPs were interacted with chemically modified gold surfaces and their interactions were monitored electrochemically. The typical experiment consisted of characterized SAMs on gold prepared from cystamine amino acid conjugates and also from 11-mercaptoundecanethiol, which were exposed to water-soluble Au NPs for a period of time, followed by rigorous washing to remove all non-specific material from the surface. Only after rinsing, the characteristics of the SAMs were studied by electrochemical and spectroscopic techniques (CV, EIS, QCM, and RAIRS).

The result presented in this thesis show for the first time that neutral and charged systems both demonstrated considerable interactions. In these systems, interactions occur between the NPs and SAMs on gold. Presumably, electrostatic attraction plays a key role in this interaction.

CV measurements for the neutral films as well as charged films exposed to anionic NPs in the presence of anionic probes in solution showed a decrease in current density, whereas the same films but exposed to cationic NPs demonstrated an increase in current density. This may be rationalized by the repulsion of the anionic probes when the anionic NPs are immobilized on the SAMs and attraction of the anionic probes when the cationic NPs are immobilized on the SAMs. The repulsion of the probes keeps them away from the electrode surface; consequently this provides less access to the electrode surface and leads to more hindrance in the charge transfer process. Conversely,

attractions of the probes facilitate mass transport by bringing them to the vicinity of the electrode surface.

The EIS data are consistent with the data resulting from the CV experiments. The apparent increase in the charge transfer resistance for the immobilized anionic NPs on the films is in agreement with the lower current density obtained from the related CV measurements. On the other hand, the dramatic decrease in the charge transfer resistance for the immobilized cationic NPs on the films indicates extensive access of the anionic probes to the electrode surface, which might be due to the attraction of the anionic probe by the cationic NPs and taking the probes down to the vicinity of the electrode surface through the active sites produced by the disturbed films. This confirms the higher amount of current density obtained in the CV measurements.

In addition, the mass increase in the QCM measurements for the diluted DT/MUA film exposed to Gly-CSA-Au NPs and the amide and other signals related to NPs in RAIR exhibited certain evidences for the existence of the NPs on the SAMs, even after rinsing with water and ethanol.

Consequently, we have demonstrated that interactions exist between charged NPs and very simple biomolecule models, both neutral and charged molecules, which have charges or at least polar groups such as carbonyl and amide groups. However, there are questions left unanswered in this research, which need to be addressed in the future:

1) The exact nature of the interaction must be evaluated in more detail. Although I was able to demonstrate in my work that there is an interaction between modified surfaces and modified Au NPs, I was not able to elucidate in detail the mechanism of the

interaction. In some cases, electrostatic interactions appear to be the major contributor, while in other there is a more specific interaction between the SAMs and the NPs, potentially H-bonding. A more detailed study should be carried out evaluating the influence of ionic strength and temperature. H-bonding is supremely sensitive to temperature and electrostatic interaction should be influenced by the presence of various anions and cations in solution, thereby giving us more information about the interaction between SAMs and NPs.

2) The molecules used as models were simple amino acid conjugates. It would be useful to explore the interaction of NPs with more complex biomolecules such as short peptide and oligonucleotide sequences. These studies might provide more insight into the interactions of NPs with biological molecules and may even allow us to answer questions such as “Does the structure of biomolecules affect the interactions with NPs?” or even “Can the interactions affect the structure of DNA or peptides?”.

4. EXPERIMENTAL

4.1. General Method and Chemicals

All reactions were carried out in dichloromethane (DCM) freshly distilled from CaH_2. All reagents, 1-ethyl-3-(3-dimethylaminopropyl) carbodiimide hydrochloride (EDC), N-hydroxybenzotriazole monohydrate (HOBt), (Boc-Gly-OH), Boc-Asp(Bz)-OH, and H-Lys(Z)-OMe.HCl, were used as received from Advanced ChemTech. Cystamine dihydrochloride (CSA), trifluoroaceticacid (TFA), and triethylamine (Et_3N) from Aldrich, magnesium sulfate ($MgSO_4$), Ferrocene from Alfa Aesar, sodium hydrogen carbonate ($NaHCO_3$), and citric acid monohydrate were purchased from EMD Chemical Inc., and were used as received. $CDCl_3$ from Cambridge Isotope Laboratories Inc. was stored over molecular sieves (8-12 mesh; 4 Å effective pore size; Fisher).

Flash column chromatography was carried out in air using 230-400 mesh silica gel (Silicycle Chemical Division). TLC were performed on aluminum plates coated with silica gel (EM Science). ^1H and $^{13}C\{^1H\}$ NMR spectra were recorded on a Bruker AMX-500 operating at 500 MHz for ^1H and 125.78 MHz for $^{13}C\{^1H\}$. ^1H and $^{13}C\{^1H\}$NMR spectra are reported in ppm relative to tetramethylsilane ($\delta = 0$) and are referenced to the residual signal of $CHCl_3$ ($\delta = 7.30$ for ^1H, $\delta = 77.23$ for $^{13}C\{^1H\}$). FT-IR spectra were collected using Bio-Rad Infra-Red Spectrometer with a resolution of 2 cm^{-1} for solid samples, and a Thermo Electron Corporation Spectrometer (Model: Nicolet NEXUS 870 FT-IR) with 2 cm^{-1} resolution for reflectance-absorbance IR studies (RAIR).

4.2. General Synthesis and Purification of Boc-peptide Disulfides

The amide coupling synthesis was carried out using the carbodiimide HOBT method[47]. Amino acid (1.0 mmol) was stirred with 1-ethyl-3-(3-dimethylaminopropyl) carbodiimide hydrochloride (EDC) (1.1 mmol), and N-Hydroxybenzotriazole monohydrate (HOBt) (1.1 mmol) in CH_2Cl_2. In a separate flask, Cystamine dihydrochloride, (0.55 mmol) was dissolved in CH_2Cl_2, using Et_3N (4.2mmol), and was added to the stirring reaction mixture after 30 minutes at 0^oC. The reaction was continued over night. The work up consisted of standard aqueous procedure of subsequently washing the reaction mixture with saturated $NaHCO_3$, citric acid (10%), saturated $NaHCO_3$ solutions followed by distilled water. The organic layer was collected and dried (using magnesium sulfate) to obtain the crude product. Column chromatography and a solvent mixture were used to purify the solid.

4.2.1 Preparation of $[Boc\text{-}Gly\text{-}CSA]_2$ (1)

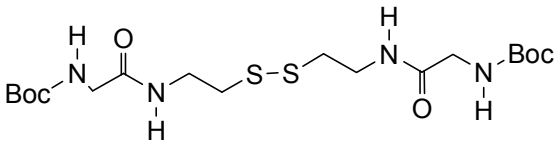

For the preparation of compound **1**, the general procedure was applied. Boc-Gly-OH (0.88 g, 5 mmol) was coupled with cystamine dihydrochloride $[CSA.HCl]_2$ (0.62 g, 2.75 mmol) in dry DCM (80 ml). Column chromatography and a solvent mixture (R_F = 0.5; 5% MeOH in EtOAc) were applied to purify the white solid. Yield = 0.96 g (82 %). ^{1}H-NMR ($CDCl_3$, δ in ppm): 6.97 (1H, br. S, NH CSA), 5.54 (1H, br. S, NH Gly), 3.85

(2H, d, $^{\alpha}CH_2$ Gly), 3.61 (2H, q, $^{\beta}CH_2$ CSA), 2.85 (2H, t, $^{\alpha}CH_2$ CSA), 1.47 (9H, s, CH_3 Boc). $^{13}C\{^1H\}$-NMR ($CDCl_3$): 170.6 (C=O, Gly), 156.6 (C=O, Boc), 80.7 (C, Boc), 44.8 (CH_2, Gly), 38.9 ($^{\beta}CH_2$, CSA), 38.4 ($^{\alpha}CH_2$ CSA), 28.7 (CH_3, Boc).

4.2.2. Preparation of [Boc-Asp(Bz)-CSA]$_2$ (2)

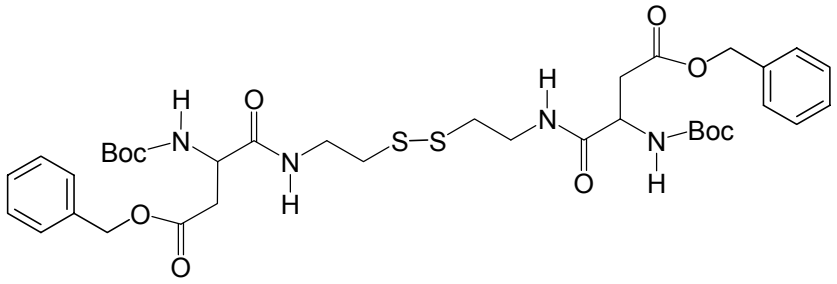

To prepare compound **2**, the general procedure was applied. Boc-Asp(Bz)-OH (0.81 g, 2.5 mmol), was coupled with cystamine dihydrochloride $[CSA.HCl]_2$ (0.285 g, 1.25 mmol) in dry DCM (150 ml). Column chromatography and a solvent mixture (R_F = 0.4; 5% MeOH in $CHCl_3$) were applied to purify the white solid. Yield = 0.78 g (82 %). ^1H-NMR (D_2O): 7.37 (5H, ph), 7.03 (1H, s, NH CSA), 5.80 (1H, s, NH Boc), 5.15 (2H, q, CH_2-ph), 4.56 (1H, $^{\alpha}CH$ Asp), 3.52 (2H, q, $^{\beta}CH_2$ CSA), 3.05 (1H, $^{\beta}CH_2$ Asp), 2.77 (2H, m, $^{\alpha}CH_2$ CSA), δ 1.47 (9H, s, Boc). $^{13}C\{^1H\}$-NMR (D_2O): 171.9 (CO, Asp), 171.5 (CO, Asp), 155.9 (CO, Boc), 135.8 (C, Bz), 128.7, 128.8, 129.0 (CH, Bz), 80.9, (C, Boc), 67.2 (CH_2, Bz), 51.0 ($^{\alpha}CH$, Asp), 38.8 ($^{\alpha}CH_2$ CSA), 37.8 ($^{\beta}CH_2$, Asp), 36.6 ($^{\beta}CH_2$ CSA), 28.7 (CH_3, Boc).

4.2.3. Preparation of Fc-Lys(Boc)-OMe (3)

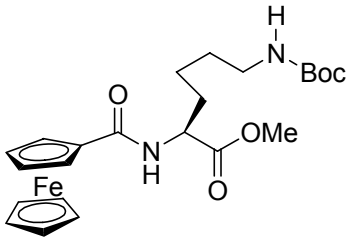

To prepare compound **3** Ferrocene carboxylic acid, which was already synthesized following literature procedure[49], (12.5 g, 5.5 mmol) and amino acid H-Lys(Boc)-OMe.HCl (1.96 g, 6.6 mmol) following the general procedure were coupled. Column chromatography and a solvent mixture (R_F = 0.75; Hexane/EtOAc 1:1) were applied to purify the orange solid product. Yield = 2.00 g (76 %). ^{1}H-NMR ($CDCl_3$): 6.21 (1H, d, $^{\alpha}$NH Lys), 4.76 (2H, CH_m Cp), 4.60 (1H, br. s, $^{\alpha}$CH Lys), 4.42 (2H, s, CH_o Cp), 4.25 (5H, s, CH unsubstit. Cp), 3.80 (3H, s, CH_3), 3.15 (2H, q, CH_2 Lys), 1.94 and 1.77 (1H, 1H, m, CH_2 Lys), 1.55 (2H, q, CH_2), 1.44 (9H, s, Ch_3 Boc), 1.42 (2H, CH_2).

4.2.4. Preparation of Fc-Lys(Boc)-OH (4)

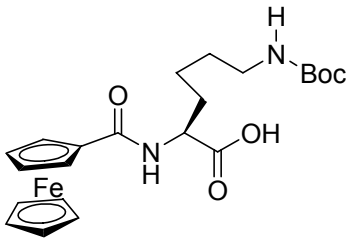

To prepare compound **4**, Fc-Lys(Boc)-OMe, compound **3**, (2.0 g, 4.2 mmol) was dissolved in dioxane (100 ml). NaOH (0.17 g, 4.2 mmol) was separately dissolved in water (1 ml) and then was added into the stirring reaction mixture. The reaction was carried out for 5 hours. The workup was done by evaporating the solvent, dissolving in water and then washing with DCM. The aqueous salt product turned into organic acid by adding concentrated hydrochloric acid to it. The organic layer was collected and dried. Yield = 1.67 g (86%).

4.2.5. Preparation of [Fc-Lys(Boc)-CSA]$_2$ (5)

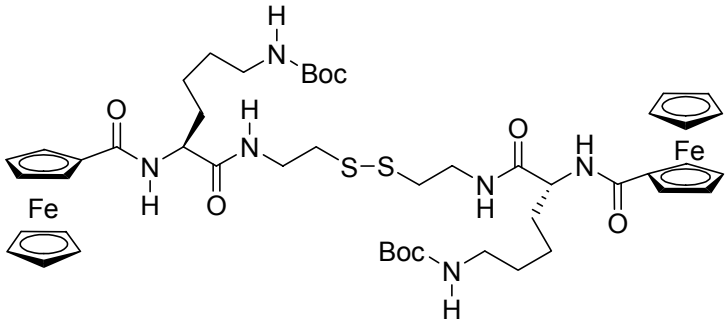

Using general procedure compound **4,** Fc-Lys(Boc)-OH, (1.93 g, 4.2 mmol), was coupled with cystamine dihyrochloride (0.56 g, 2.5 mmol) to produce compound **5**. Column chromatography and a solvent mixture (R_F = 0.3; 25% Hexane in EtOAc) was applied to purify the orange solid. Yield = 1.78 g (82 %). MW calculated for $C_{48}H_{68}N_6O_8Fe_2S_2$ = 1032.3239; HR-MS (FAB): found = 1033.3362 $[M+1]^+$.

^{1}H-NMR ($CDCl_3$): 7.58 (NH CSA), 7.05 ($^{\alpha}$NH Lys), 5.05 (NH, Boc), 4.92 (1H, $^{\alpha}$CH Lys), 4.84 (2H, CH_o Cp), 4.38 (2H, s,CH_m Cp), 4.22 (5H, s, unsubstit. Cp), 3.78 and 3.45 ((1H, 1H, $^{\beta}CH_2$ CSA), 3.22 and 3.15 (1H, 1H, CH_2 Lys), 2.82 (2H, s, $^{\alpha}CH_2$

CSA), 1.93 (2H, m, CH_2 Lys), 1.56 (2H, q, CH_2 Lys), 1.50 (2H, CH_2 Lys)1.44 (9H, s, Ch_3 Boc). ^{13}C-NMR ($CDCl_3$): 173.8 (CO, Lys), 171.9 (CO, Fc), 156.6 (CO, Boc), 79.7 (C, Boc), 71.3 (C_i, Fc), 70.3-68.9 (CH, Fc), 53.2 ($^{\alpha}$CH, Lys), 40.5(CH_2, Lys), 38.9 ($^{\beta}CH_2$, CSA), 38.5 ($^{\alpha}CH_2$, CSA), 32.1 (CH_2, Lys), 30.1 (CH_2, Lys), 28.8 (CH_3, Boc), 23.4 (CH_2, Lys).

4.3. Electrochemical measurements

The electrochemical experiments were carried out at room temperature (23 ± 2^{oC}) using CHI 660b (Instrument Inc.). The QCM measurements were performed by using CHI 440 (Instrument Inc.). A gold electrode (BAS, diameter 1.6 mm) was used as working electrode and Pt wire as counter electrode while Ag/AgCl (BAS) was used as a reference electrode. A glassy carbon electrode (BAS, diameter 2 mm) was also used as working electrode for electrochemical characterization of compound **5**. The electrodes were cleaned through the cleaning process and then were used for the modification and electrochemical measurement purposes.

4.3.1. Cleaning the Electrodes

Electrodes were always cleaned just before modification through a process of cleaning. To clean an electrode, they were polished on slurry of alumina 3 μm followed by 1 μm, then 0.5 μm alummina in sequence. Then they were electrochemically cleaned in a 0.5 M KOH by applying a linear sweep voltammetry (LSV) in the potential range of

0.0 to -1.4 V versus Ag/AgCl at a scan rate of 100 mV/s. The gold electrodes were then subjected to cyclic voltammetry (CV), sweeps between 0.0 and 1.6V vs Ag/AgCl at a scan rate of 100 mV/s in 0.5 M H_2SO_4 solution, until a stable CV was obtained.

4.3.2. Preparation of Films

Cleaned electrodes were immersed in 1 mM ethanolic solutions of peptide disulfides. The electrodes were soaked in this solution for 5 days or in the case of alkanethiol for a range of time from 12 hours to a maximum of 2 days. Finally, the electrode was rinsed with copious amount of absolute ethanol followed by Milli-Q water and then dried with a stream of nitrogen.

Alternatively, an electrochemichal deposition method was used with identical results. A potential of -1.3 V, (*vs* Ag/AgCl) was applied to the clean electrodes in 10 mM ethanolic solution of peptide disulfide for 30 minutes. Then, the electrodes were sonicated in ethanol for maximum 2 minutes and then rinsed with large amount of absolute ethanol, followed Milli-Q water. For both methods, leaving the modified electrodes in Milli-Q water for 5 or 6 hours produced better results, most likely because of better organization of the molecules on surface.

4.3.3. Blocking Studies

Blocking studies were carried out on BAS gold electrodes modified with compounds **1**, **3**, **6**, and 11-mercaptoundecanoic acid (MUA) by applying CV experiments at room temperature (23 ± 2^{oC}) in an equimolar solution of 1 mM $[Fe(CN)_6]^{3-}$/$[Fe(CN)_6]^{4-}$, in 50 mM phosphate buffer (2.9 g/L, NaH_2PO_4 and 4.1 g/L,

Na_2HPO_4, pH = 7.0). All CVs were carried out at 100 mV/s scan rate, unless otherwise mentioned.

4.3.4. Solution Electrochemistry

CV studies of compound (**6)** were carried out at room temperature (23 ± 2^{oC}). Freshly distilled acetonitrile (from CaH_2) was used as solvent and 0.1 M tetrabutylammonium perchlorate (TBAP) as supporting electrolyte. Glassy carbon working electrode (BAS, diameter 3 mm), and platinum wire counter electrode were used along with Ag/AgCl in 3 M KCl (BAS) as reference electrode. IR compensation and a 100 mV/s scan rate were applied to record the voltammograms over the range of 0 to 700 mV.

4.3.5. Quartz Crystal Microbalence (QCM) measurements

Using CHI 440 (CH Instruments Inc.), quartz crystal microbalance measurments were carried out on quartz crystals (8 MHz, AT-cut, 0.205 cm^2 area) covered with Au (1000 Å) on a Ti adhesion layer (100 Å), commercially available from CH Instruments. In a QCM experiment frequency changes of the crystal are directly measured. Then, based on the measured frequency changes, the mass changes on the surface of the crystal are calculated using Sauerbrey equation (Eq. 1):

$$\Delta f = \frac{-2 f_0^{\,2}}{A\sqrt{\mu\rho}}\Delta m \qquad (1)$$

Where f_0 is the resonant frequency of the fundamental mode of the crystal, A the area of the gold disk coated onto the crystal (0.205 cm^2 for given crystal), ρ is the density (2.648 g/cm^3), and μ is the shear modulus of the quartz crystal (2.947 x 10^{11} $g/cm\ s^2$). For 8 MHz crystal, the mass change is 0.14 ng for 0.1 Hz frequency change.

Preparation of monolayer on the crystal surface was analogous to that explained above for other surfaces. The crystals were rinsed with absolute ethanol and immediately soaked in 1 mM ethanolic solution of MUA for 2 days, followed by washing with ethanol and Milli-Q water and drying under a stream of nitrogen. A QCM experiment was carried out on the modified crystal using 50 mM phosphate buffer solution (2.9 g/L, NaH_2PO_4 and 4.1 g/L, Na_2HPO_4, pH = 7.0). 200 µL solution of Gly-CSA-Au NPs was *in situ*. injected into the QCM cell at 550s, when a stable signal was observed.

4.4. FT-IR Spectroscopy

Solid state FT-IR experiments were carried out using Bio-Rad Infra-red Spectrometer. Compound **1**, and **2** were mixed and crushed with KBr pollet, and then the spectra were recorded with 256 scans. A mixed film of MUA / $C_{10}SH_{22}$ on gold surface was studied by reflectance-absorbance FT-IR spectroscopy (RAIR). Clean gold substrates, Au on Si (100) (Platypus Technologies, Inc) wafers, were soaked in 1 mM ethanolic solution of MUA / $C_{10}SH_{22}$ with a 1:3 molar ratio, respectively. The modified surfaces were rinsed with ethanol and Milli-Q water after one day and then the FT-IR spectra were collected (2000). All RAIR spectra were collected at an angle of 78^o of the

incidence IR beam at 2 cm^{-1} resolution and wavelength window between 1250 and 3700 cm^{-1}.

4.5. X-ray Photoelectron Spectroscopy (XPS)

XPS was carried out on Kratos (AEI) DS300 instrument, using the Mg K lines for excitation at the University of Alberta. The specimen was mounted on a double-stick scotch tape. The position of core levels was calibrated relative to the gold $4f_{7/2}$ line (assumed to be at 83.8 eV). Samples were prepared by treating the gold substrate (commercially available from CH Instruments Inc.) with piranha solution (70% conc. H_2SO_4 + 30% H_2O_2). **Caution: Piranha solution is highly oxidizing and any direct contact should be avoided**) to remove any organic contaminants. Then, it was washed with copious amount of water followed by ethanol, dried over argon and then soaked in a 1 mM ethanolic solution of MUA for 2 days. All substrates were stored in an atmosphere of argon before doing the XPS measurements.

5. REFERENCES

(1) Eustis, S.; El-Sayed, M. A. *Chem. Soc. Rev.* **2006**, *35*, 209-217.
(2) Diederich, F.; Whetten, R. L. *Angew. Chem. Int. Ed.* **1991**, *30*, 678-680.
(3) O. P. Gorelik, O. P.; Dyuzhev, G. A.; Novikov, D. V.; Oichenko, M. O.; Fursei, G. N. *TECHNICAL PHYSICS* **2000**, *45*, 1489–1495.
(4) Roco, M. C. *Journal of Nanoparticle Research* **1999**, *1*, 1-6.
(5) Michalet, X.; Pinaud, F. F.; Bentolia, L. A.; Tsay, J. M.; Doose, S.; Li, J. J.; Sundaresan, G.; Wu, A. M.; Gambhir, S. S.; Weiss, S. *Science* **2005**, *307*, 538-544.
(6) Bruchez, M.; Moronne, M.; Gin, P.; Weiss, S.; Alivisatos, A. P. *Science* **1998**, *281*, 2013-2016.
(7) Chan, W. C. W.; Nie, S. M. *Science* **1998**, *281*, 2016-2018.
(8) http://www.nutralease.com/index.asp.
(9) http://www.iogear.com/...27RW6.
(10) http://www.advancednanotechnology.com/zinclear.php.
(11) Oberdörster, G. *Philos. Trans. R. Soc. London, Ser. A* **2000**, *358*, 2719-2740.
(12) Warheit, D. B. *Mater. Today* **2004**, *7*, 32-35.
(13) Donaldson, K.; Stone, V.; Clouter, A.; Renwick, L.; MacNee, W. *Occup. Environ. Med.* **2001**, *58*, 211-216.
(14) Borm, P. J. A.; Kreyling, W. *J. Nanosci. Nanotech.* **2004**, *4*, 521-531.
(15) Whitesides, G. M. *Small* **2005**, *1*, 172-179.
(16) Warheit, D. B.; coworker *Toxicologist* **2003**, *72*, 298.
(17) Conner, E. E.; Mwamuka, J.; Gole, E.; Murphy, C. J.; Wyatt, M. D. *Small* **2005**, *1*, 325-327.
(18) Murray, C. B.; Norris, D. J.; Bawendi, M. G. *J. Am. Chem. Soc.* **1993**, *115*, 8706-8715.
(19) Wang, W.; Germanenko, I.; El-Shall, M. S. *Chem. Mater. 2002, 14, 3028-3033*
2002, *14*, 3028-3033.
(20) Brust, M.; Walker, M.; Bethell, D.; Schiffrin, D. J.; Whyman, R. *J. CHEM. SOC., CHEM. COMMUN.* **1994**, 801-802.
(21) Brust, M.; Fink, J.; Bethella, D.; Schiffrina, D. J.; Kiely, C. *J. CHEM. SOC., CHEM. COMMUN.* **1995**, 1655-1656.
(22) Warheit, D. B.; Laurence, B. R.; Roach, D. H.; Reynold, G. A.; Webb, T. R. *Toxical Sci.* **2003**, *77*, 117-125.
(23) Nuzzo, R. G.; allara, D. *J. Am. Chem. SOC.* **1983**, *105*, 4481-4483.
(24) Nuzzo, R. G.; Dubois, L. H.; Allara, D. L. *J. Am. Chem. Soc* **1990**, *112*, 558-559.
(25) Allara, D. L.; Nuzzo, R. G. *Langmuir* **1985**, *1*, 45.
(26) Allara, D. L.; Nuzzo, R. G. *Langmuir* **1985**, *1*, 52.
(27) Bain, C. D.; Troughton, E. B.; Tao, Y.-T.; Evall, J.; Whitesides, G. M.; Nuzzo, R. G. *J. Am. Chem. Soc.* **1989**, *111*, 321-335.
(28) Bain, C. D.; Whitesides, G. M. *Angew. Chem. Int. Ed.* **1989**, *28*, 506-512.
(29) Bain, C. D.; Biebuyck, H. A.; Whitesides, G. M. *Langmuir* **1989**, *5*, 723.

(30) Bain, C. D.; Whitesides, G. M. *J. Am. Chem. Soc.* **1989**, *93*, 1970-1973.
(31) Biebuyck, H. A.; Bain, C. D.; Whitesides, G. M. *Langmuir* **1994**, *10*, 1825-1831.
(32) Ulman, A. *Chem. Rev.* **1996**, *96*, 1533-1554.
(33) Appoh, F. E.; Long, Y.-T.; Kraatz, H.-B. *Langmuir* **2006**, *22*, 10515-10522.
(34) Yang, W. R.; Hibbert, D. B.; Zhang, R.; Willet, G. D.; Gooding, J. J. *Langmuir* **2005**, *21*, 260-265.
(35) Zamborini, F. P.; Hicks, J. F.; Murray, R. W. *J. Am. Chem. Soc.* **2000**, *122*, 4514-4515.
(36) Zhao, J.; Bradbury, C. R.; Huclova, S.; Potapova, I.; Carrara, M.; Fermin, D. *J. Phy. Chem. B* **2005**, *109*, 22985-22994.
(37) Porter, M. D.; Bright, T. B.; Allara, D.; Chidsey, C. E. D. *J. Am. Chem. Soc.* **1987**, *109*, 3559-3568.
(38) Ganesh, V.; Pal, S. K.; Kumar, S.; Lakshminarayanan, V. *Journal of Colloid and Interface Science* **2006**, *296*, 195-203.
(39) Cheng, I. F.; Whiteley, L. D.; Martin, C. R.; Chem., A. **1989**, *61*, 762.
(40) Finklea, H. O.; Snider, D. A.; Fedyk, J.; Sabatani, E.; Gafni, Y.; Rubinstein, I. *Langmuir* **1993**, *9*, 3660.
(41) Protsailo, L. V.; Fawcett, W. R. *Langmuir* **2002**, *18* 8933.
(42) Katz, E.; Willner, I. *Electroanalysis* **2003**, *15*, 913-946.
(43) Ding, S.-J.; Changb, B.-W.; Wu, C.-C.; Lai c, M.-F.; Changc, H.-C. *Analytica Acta* **2005**, *554*, 43-51.
(44) Qingwen, L.; Hong, G.; Yiming, W.; Guoan, L.; Jie, M. *Electroanalysis* **2001**, *13*, 1342-1346.
(45) Kraatz, H.-B.; Bediako-Amoa, I.; Gyepi-Garbrah, S. H.; Sutherland, T. C. *J. Phys. Chem. B.* **2004**, *108*, 20164-20172.
(46) Appoh, F. E.; Sutherland, T. C.; Kraatz, H.-B. *Journal of Organometallic Chemistry* **2005**, *690* 1209–1217.
(47) König, W.; Geiger, R. *Chem. Ber.* **1970**, *103*, 788-798.
(48) Chidsey, C. E. D.; Bertozzi, C. R.; Putvinski, T. M.; Mujsce, A. M. *J. Am. Chem. Soc.* **1990**, *112*, 4301-4306.
(49) Rosenblum, M.; Woodward, R. B. *J. Am. Chem. Soc.* **1958**, *80*, 5443-5449.
(50) Rinehart, K. L.; Motz, K. L.; Moon, S. **1956**, *79*, 2749-2754.
(51) Appoh, F. E.; Thomas, D. S.; Kraatz, H.-B. *Macromolecules* **2006**, *39*, 5629-5638.
(52) Bediako-Amoa, I.; Sutherland, T. C.; Li, C.-Z.; Silerova, R.; Kraatz, H.-B. *J. Phys. Chem. B.* **2004**, *108*, 704-714.
(53) Orlowski, G. A.; Chowdhury, S.; Long, Y.; Kraatz, H.-B. *Chem. Commun.* **2005**, 1330-1332.
(54) Walczak, M. W.; Chung, C.; Stole, S. M.; Widrig, C. A.; Porter, M. D. *J. Am. Chem. Soc.* **1991**, *113*.
(55) Finklea, H. O. *Electrochemistry of Organized Monolayers of Thiols and related Molecules on Electrodes*; Marcel Dekker, Inc: Newyork, 1996; Vol. 19.

(56) Gyepi-Garbrah, S. H.; Silerova, R. *Phys. Chem. Chem. Phys.* **2001**, *3*, 2117-2123.
(57) Cecchet, F.; Rudolf, P.; Rapino, S.; Margotti, M.; Paolucci, F.; Baggerman, J.; Brouwer, A. M.; Kay, E. R.; Wong, J. K. Y.; Leigh, D. A. *J. Phys. Chem. B.* **2004**, *108*, 15192-15199.
(58) Chen, H.; Henga, C. K.; Puiub, P. D.; Zhoub, X. D.; Leec, A. C.; Limc, T. M.; Tan, S. N. *Analytica Acta* **2005**, *554*, 52-54.
(59) Cho, Y.; Ivanisevic, A. *J. Phy. Chem. B* **2005**, *109*, 6225-6232.
(60) Cecchet, F. e. a.; Pilling, M.; Hevesi, L.; Schergna, S.; Wong, J. K. Y.; Clarkson, G. J.; Leigh, D. A.; Rudolf, P. *J. Phy. Chem. B* **2003**, *107*, 10863-10872.
(61) Liu, D.; Szulczewski, G. J.; Kispert, L. D.; Primak, A.; Moore, T. A.; Moore, A. L.; Gust, D. *J. Phy. Chem. B* **2002**, *106*, 2933-2936.
(62) Yanagida, M.; Kanai, T.; X.-Q., Z.; Kondo, T.; Uosaki, K. B. *Chem. Soc. Jpn.* **1998**, *71*, 2555-2559.
(63) Laibinis, P. L.; Bain, C. D.; Whitesides, G. M. *J. Phys. Chem. B.* **1991**, *95*, 7017-7021.
(64) Mendoza, S. M.; Arfaoui, I.; Zanarini, S.; Paolucci, F.; Rudolf, P., 23, 582-588 *Langmuir* **2007**, *23*, 582-588.
(65) Krause, P. F.; Katon, J. E.; Rogers, J. M.; Phillips, D. B. *Appl. Spectrosc.* **1977**, *31*, 110-15.
(66) Wells, M.; Dermody, D. L.; Yang, H. C.; Kim, T.; Crooks, R. M. *Langmuir* **1996**, *12*, 1989-1996.
(67) Smith, E. L.; Alves, C. A.; Anderegg, J. W.; Porter, M. D. *Langmuir* **1992**, *8*, 2707-2714.
(68) Nakayama, D.; Nishio, Y.; Watanabe, M. *Langmuir* **2003**, *19*, 8542-8549.
(69) Me´thivier, C.; Beccard, B.; Pradier, C. M. *Langmuir* **2003**, *19*, 8807-8812.
(70) Barreira, S. V. P.; Silva, F. *Langmuir* **2003**, *19*, 10324-10331.
(71) Burgess, I.; Seivewright, B.; Lennox, R. B. *Langmuir* **2006**, *22*, 4420-4428.
(72) Schweiss, R.; Welzel, P. B.; Werner, C.; Knoll, W. *Langmuir* **2001**, *17*, 4304-4311.
(73) Dai, Z.; Ju, H. *Phys. Cmeh. Chem. Phys.* **2001**, *3*, 3769-3773.
(74) Van der Vegte, E. W.; Hadziioannou, G. *J. Phy. Chem. B* **1997**, *101*, 9563-9569.
(75) Holmes-Farley, S. R.; Bain, C. D.; Whitesides, G. M. *Langmuir* **1988**, *4*, 921.
(76) Holmes-Farley, S. R.; Reamy, R. H.; McCarthy, T. J.; Deutch, J.; Whitesides, G. M. *Langmuir* **1985**, *1*, 725.
(77) Chen, S.; Yao, H.; Kimura, K. *Langmuir* **2001**, *17*, 733-739.
(78) Sun, L.; Crooks, R. M.; Rico, A. J. *Langmuir* **1993**, *9*, 1775-1780.
(79) Jiang, P.; Liu, Z. F.; Cai, S. M. *Langmuir* **2002**, *18*, 4495-44-99.
(80) Clark, R. A.; Bowden, E. F. *Langmuir* **1997**, *13*, 559-565.

APPENDIX

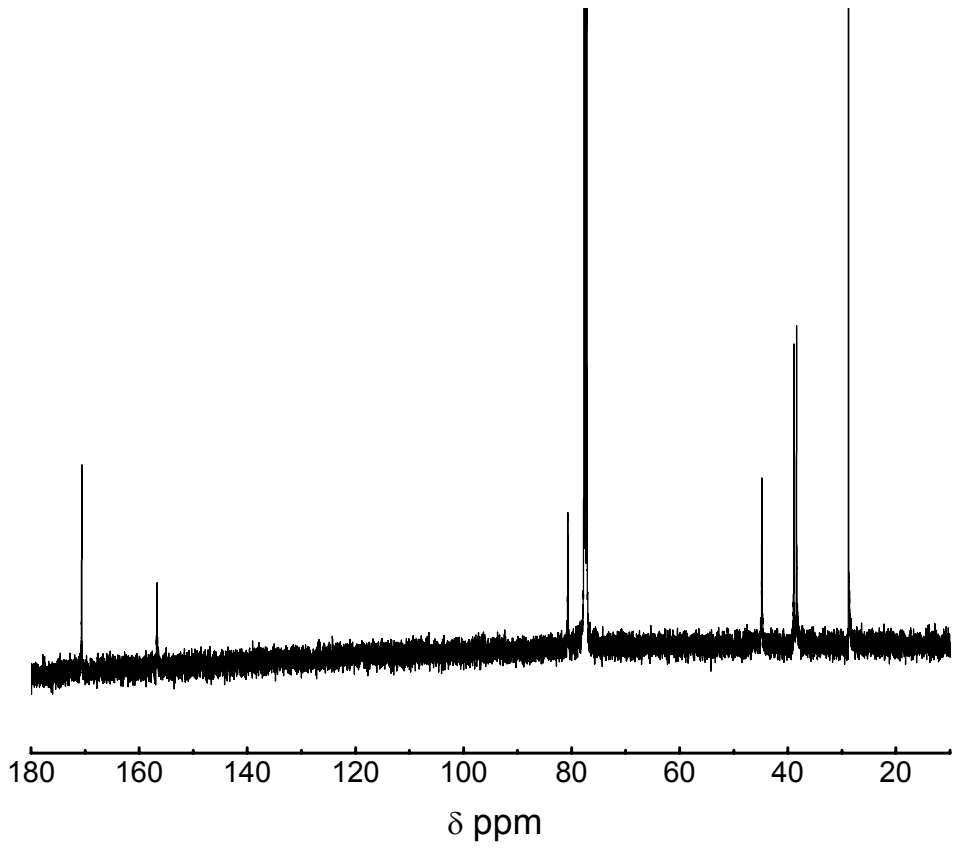

Figure 1: $^{13}C\{^{1}H\}$-NMR spectrum of compound **1** in $CDCl_3$

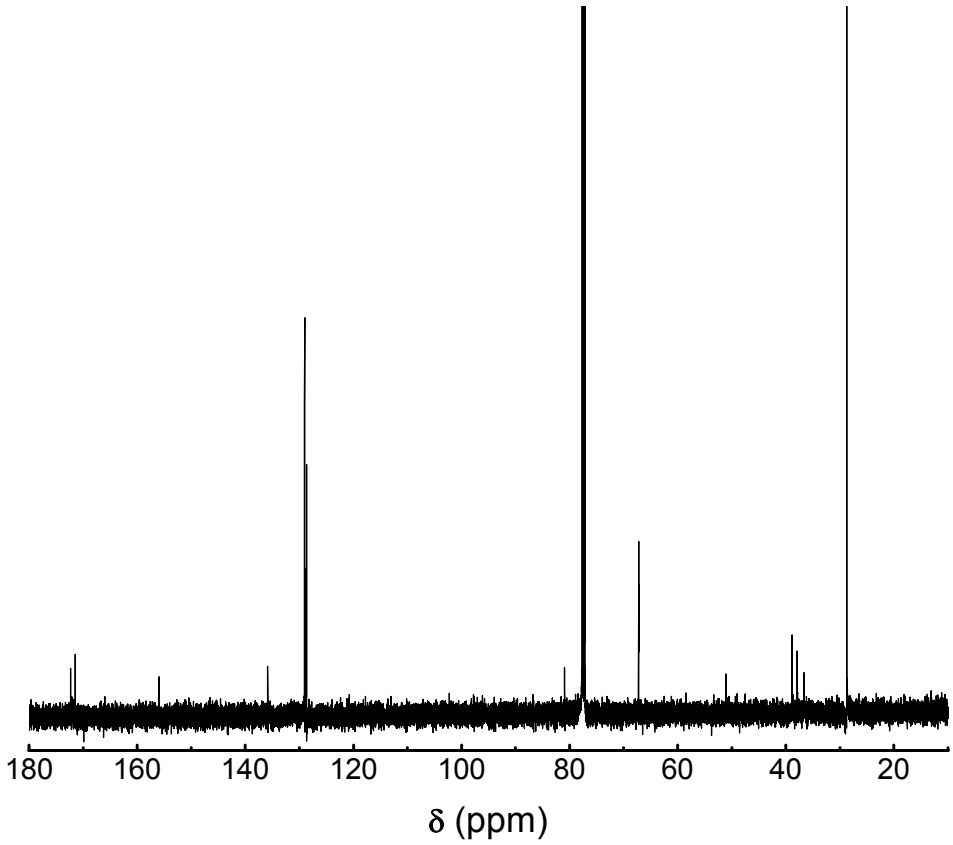

Figure 2: $^{13}C\{^{1}H\}$-NMR spectrum of compound **2** in $CDCl_3$

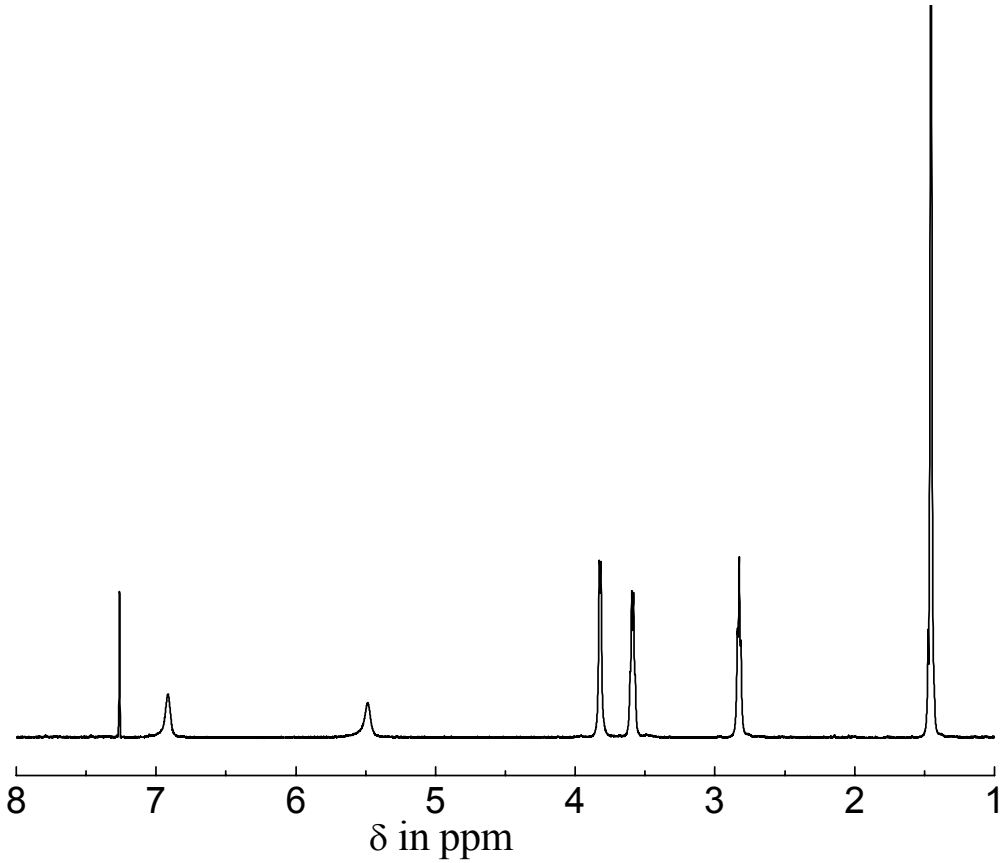

Figure 3: ^{1}H-NMR spectrum in the range of 8 – 1 ppm for compounds **1**. The spectrum was recorded in $CDCl_3$ and were referenced against the residual signal for $CHCl_3$ at δ7.23.

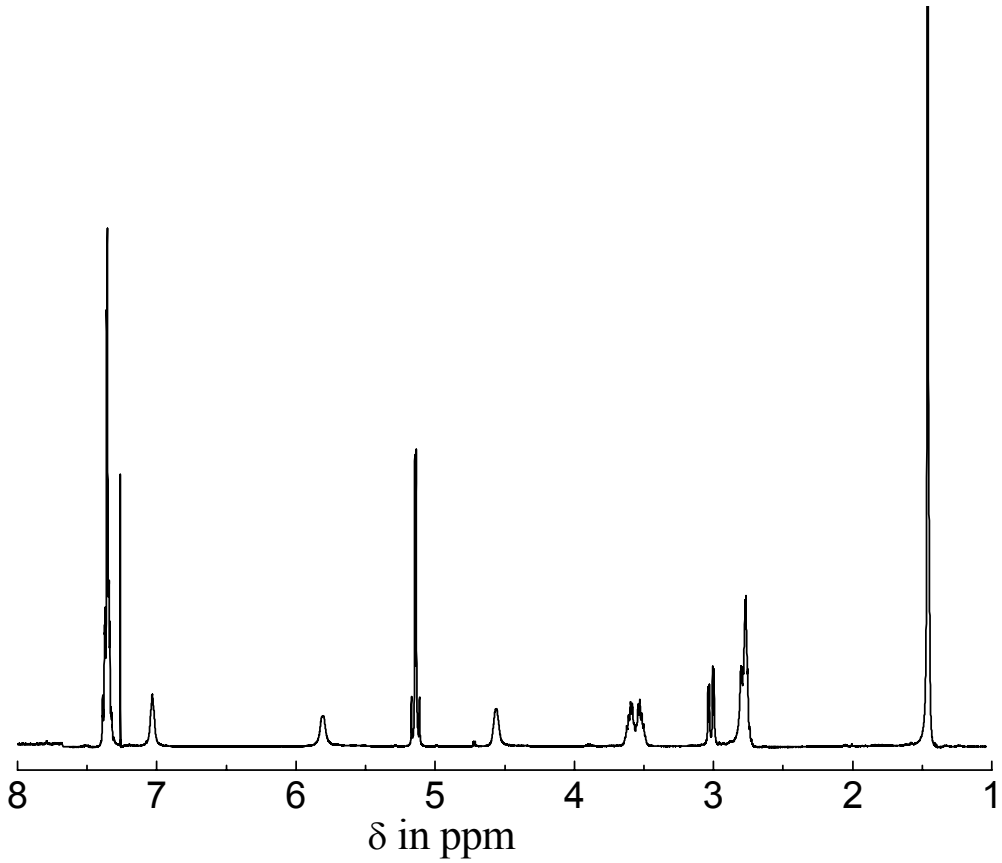

Figure 4: ^{1}H-NMR spectrum in the range of 8 – 1 ppm for compounds **2**. The spectrum was recorded in $CDCl_3$ and were referenced against the residual signal for $CHCl_3$ at δ7.23.

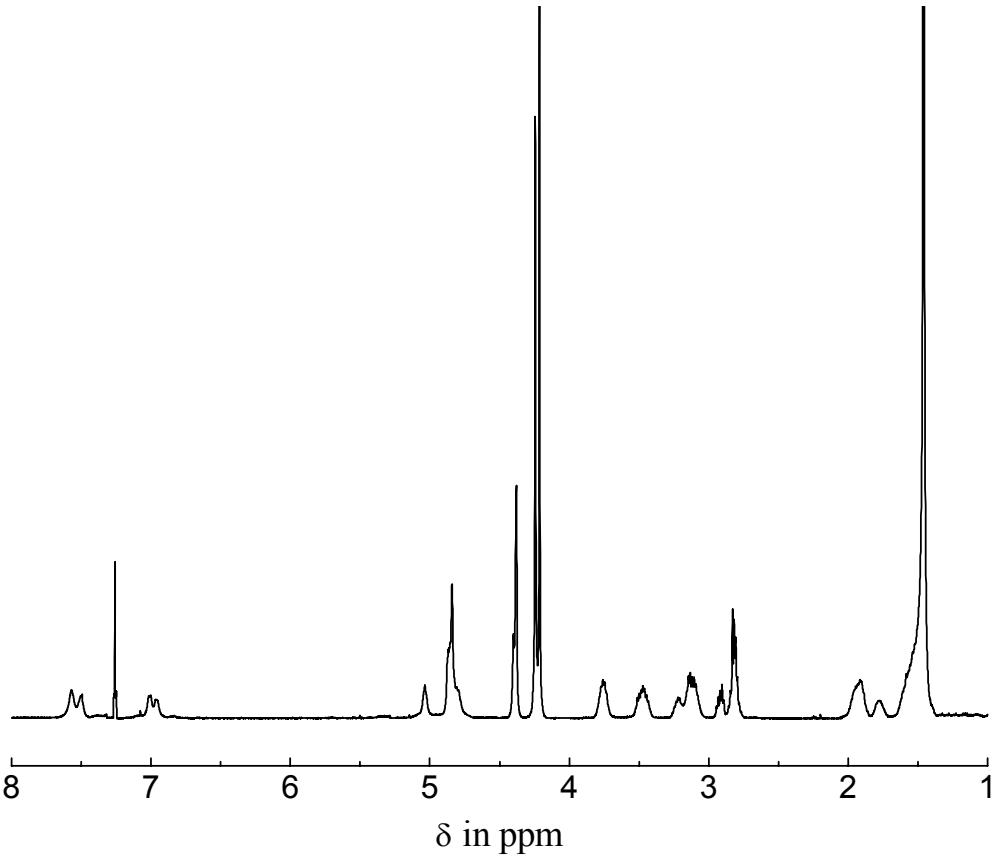

Figure 5: ^{1}H-NMR spectrum in the range of 8 – 1 ppm for compounds **5**. The spectrum was recorded in $CDCl_3$ and were referenced against the residual signal for $CHCl_3$ at δ7.23.

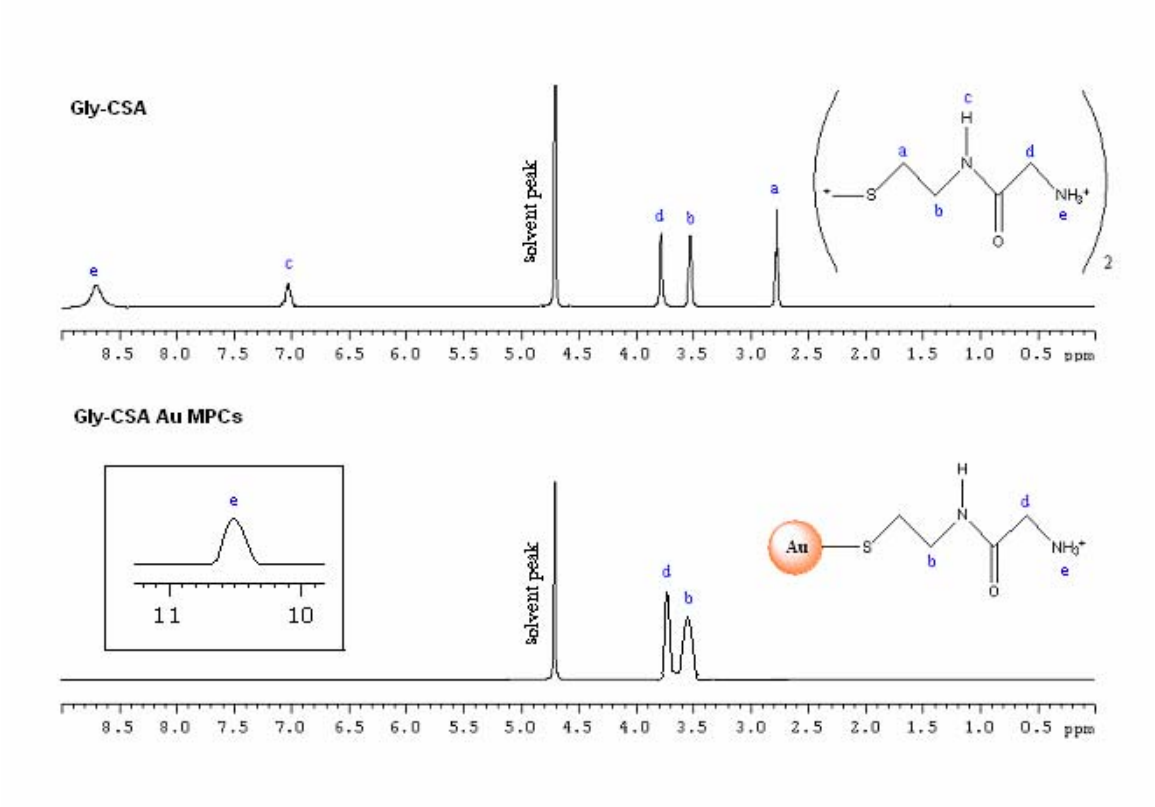

Figure 6: NMR spectrum of free Gly-CSA and Gly-CSA Au MPCs in D_2O.

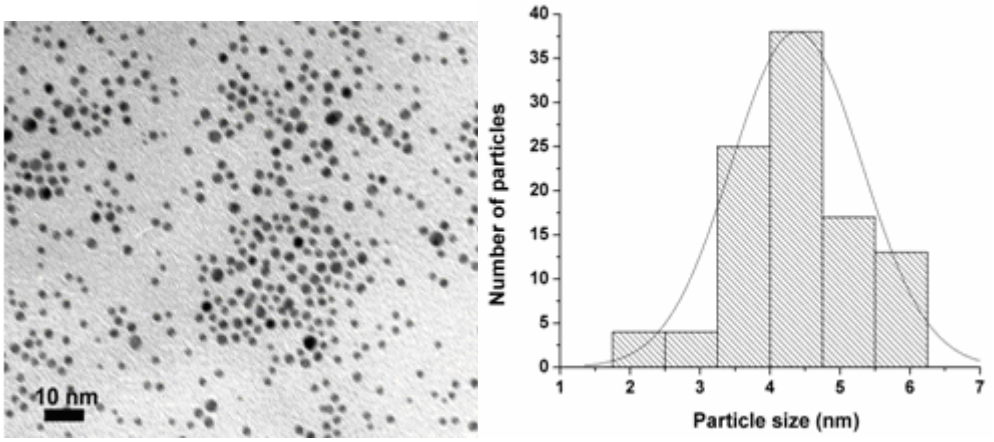

Figure 7. TEM images and size distribution histograms of Gly-CSA-Au NPs.

Copy Write Permissions

PERMISSION REQUEST FORM

Date: September 10, 2007

To: Copyright Office
Publications Division
American Chemical Society
1155 Sixteenth Street, N.W.
Washington, DC 20036

FAX: 202-776-8112

From: Amir Kavianpour
Department of Chemistry
University of Saskatchewan
110 Science Place
Saskatoon, SK S7N 5C9 Canada
Tel: (306) 966-4655 Fax:
Your Phone No. (306) 934-3853
Your Fax No. (306) 966-4730

I am preparing a paper entitled:
to appear in a (circle one) book, magazine, journal, proceedings, other
Thesis entitled: "A study on possible interactions between biomolecules and nanoparticles" to be published by:
University of Saskatchewan

I would appreciate your permission to use the following ACS material in print and other formats with the understanding that the required ACS copyright credit line will appear with each item and that this permission is for only the requested work listed above:

From ACS journals or magazines (for ACS magazines, also include issue no.):

ACS Publication Title	Issue Date	Vol.	No.	Page(s)	Material to be used*
J. Am. Chem. Soc.	1987	*109*	*(12)*	*3559-3568*	Fig.5
J. Am. Chem. Soc.	1993	*115*	(19)	8706-8715	Fig.6

From ACS books: include ACS book title, series name and number, year, page(s), book editor●s name(s), chapter author's name(s), and material to be used, such as Figs. 2 & 3, full text, etc.*

* If you use more than three figures/tables from any article and/or chapter, the author's permission will also be required.

Questions? Please call Arleen Courtney at (202) 872-4368 or use the FAX number above.

This space is reserved for ACS Copyright Office Use

PERMISSION TO REPRINT IS GRANTED BY THE AMERICAN CHEMICAL SOCIETY

ACS CREDIT LINE REQUIRED. Please follow this sample: Reprinted with permission from (reference citation). Copyright (year) American Chemical Society.

APPROVED BY: C. Arleen Courtney 9/14/07
ACS Copyright Office

☐ **If box is checked, author permission is also required. See original article for address.**

12/3/99

ELSEVIER LIMITED LICENSE TERMS AND CONDITIONS

Sep 11, 2007

This is a License Agreement between Amir Kavianpour ("You") and Elsevier Limited ("Elsevier Limited"). The license consists of your order details, the terms and conditions provided by Elsevier Limited, and the payment terms and conditions.

License Number	1785560521185
License date	Sep 10, 2007
Licensed content publisher	Elsevier Limited
Licensed content publication	Journal of Colloid and Interface Science
Licensed content title	Self-assembled monolayers (SAMs) of alkoxycyanobiphenyl thiols on gold—A study of electron transfer reaction using cyclic voltammetry and electrochemical impedance spectroscopy
Licensed content author	V. Ganesh, Santanu Kumar Pal, Sandeep Kumar and V. Lakshminarayanan
Licensed content date	1 April 2006
Volume number	296
Issue number	1
Pages	9
Type of Use	Thesis / Dissertation
Portion	Figures/table/illustration/abstracts
Quantity	2
Format	Both print and electronic
You are an author of the Elsevier article	No
Are you translating?	No
Purchase order number	
Expected publication date	Oct 2007
Elsevier VAT number	GB 494 6272 12
Permissions price	0.00 USD
Value added tax 0.0%	0.00 USD
Total	0.00 USD

Terms and Conditions

INTRODUCTION

The publisher for this copyrighted material is Elsevier. By clicking "accept" in connection with completing this licensing transaction, you agree that the following terms and conditions apply to this transaction (along with the Billing and Payment terms and conditions

ELSEVIER LIMITED LICENSE
TERMS AND CONDITIONS

Sep 11, 2007

This is a License Agreement between Amir Kavianpour ("You") and Elsevier Limited ("Elsevier Limited"). The license consists of your order details, the terms and conditions provided by Elsevier Limited, and the payment terms and conditions.

License Number	1785550856057
License date	Sep 10, 2007
Licensed content publisher	Elsevier Limited
Licensed content publication	Electrochimica Acta
Licensed content title	Electrochemical evaluation of avidin–biotin interaction on self-assembled gold electrodes
Licensed content author	Shinn-Jyh Ding, Bin-Wha Chang, Ching-Chou Wu, Min-Feng Lai and Hsien-Chang Chang
Licensed content date	10 June 2005
Volume number	50
Issue number	18
Pages	7
Type of Use	Thesis / Dissertation
Portion	Figures/table/illustration/abstracts
Quantity	2
Format	Both print and electronic
You are an author of the Elsevier article	No
Are you translating?	No
Purchase order number	
Expected publication date	Oct 2007
Elsevier VAT number	GB 494 6272 12
Permissions price	0.00 USD
Value added tax 0.0%	0.00 USD
Total	0.00 USD

Terms and Conditions

INTRODUCTION

The publisher for this copyrighted material is Elsevier. By clicking "accept" in connection with completing this licensing transaction, you agree that the following terms and conditions apply to this transaction (along with the Billing and Payment terms and conditions

From "CONTRACTS-COPYRIGHT (shared)" <Contracts-Copyright@rsc.org>
Sent Tuesday, September 11, 2007 0:33 am
To ahk155@mail.usask.ca
Cc
Bcc
Subject RE: Permission Request Form: Amir Kavianpour

Dear Mr Kavianpour

The Royal Society of Chemistry hereby grants permission for the use of the material specified below in the work described and in all subsequent editions of the work for distribution throughout the world, in all media including electronic and microfilm. You may use the material in conjunction with computer-based electronic and information retrieval systems, grant permissions for photocopying, reproductions and reprints, translate the material and to publish the translation, and authorize document delivery and abstracting and indexing services. The Royal Society of Chemistry is a signatory to the STM Guidelines on Permissions (available on request).

Please note that if the material specified below or any part of it appears with credit or acknowledgement to a third party then you must also secure permission from that third party before reproducing that material.

Please ensure that the published article carries a credit to The Royal Society of Chemistry in the following format:

[Original citation] – Reproduced by permission of The Royal Society of Chemistry

and that any electronic version of the work includes a hyperlink to the article on the Royal Society of Chemistry website. The recommended form for the hyperlink is http://dx.doi.org/10.1039/*DOI suffix*, for example in the link http://dx.doi.org/10.1039/b110420a the DOI suffix is 'b110420a'.

Regards

Gill Cockhead
Contracts & Copyright Executive

Gill Cockhead (Mrs), Contracts & Copyright Executive
Royal Society of Chemistry, Thomas Graham House
Science Park, Milton Road, Cambridge CB4 0WF, UK
Tel +44 (0) 1223 432134, Fax +44 (0) 1223 423623
http://www.rsc.org

-----Original Message-----
From: ahk155@mail.usask.ca [mailto:ahk155@mail.usask.ca]
Sent: 11 September 2007 00:04
To: CONTRACTS-COPYRIGHT (shared)
Subject: Permission Request Form: Amir Kavianpour

Name : Amir Kavianpour
Address :

Department of Chemistry
University of Saskatchewan
110 Science Place
Saskatoon, SK S7N 5C9 Canada

Tel : 306-934-3853
Fax : 306-966-4730
Email : ahk155@mail.usask.ca

I am preparing the following work for publication:

Article/Chapter Title : A study on possible interactions between biomolecules and nanoparticles
Journal/Book Title : M. Sc. Thesis
Editor/Author(s) : Amir Kavianpour
Publisher : University of Saskatchewan

I would very much appreciate your permission to use the following material:

Journal/Book Title : J. CHEM. SOC., CHEM. COMMUN
Editor/Author(s) : M. Brust, et al.
Volume Number :
Year of Publication : 1995
Description of Material : Fig.2 (a and b) on page- 1656
Page(s) : 1655-1656

Any Additional Comments :